Isyna Izzal Muna, M.Sc.

Institute of Fluid Flow Machinery, Polish Academy of Sciences
Mechanics of Intelligent Structures Department

DEGRADATION OF ADDITIVELY MANUFACTURED POLYMER BASED COMPOSITES UNDER THERMAL CONDITIONS

A dissertation submitted to the Scientific Board of Institute of Fluid Flow Machinery,
Polish Academy of Sciences in partial fulfillment of the requirements
for the Degree of Doctor of Philosophy

Supervisor:
Magdalena Mieloszyk, D.Sc. Ph.D. Eng.

June, 2024

ACKNOWLEDGMENTS

First and foremost, I would like to express my sincere gratitude to my supervisor, D.Sc Ph.D Eng. Magdalena Mieloszyk. Her guidance, patience, and unwavering support have been instrumental in my journey. Your insightful feedback and encouragement have helped shape this work, and I am deeply thankful for the knowledge and wisdom you have shared with me.

I am also immensely grateful to all of my colleagues and friends at IMP PAN, Gdansk, Poland. Your camaraderie, collaboration, and kindness have made this journey not only academically enriching but also personally fulfilling.

To my beloved parents, I owe a debt of gratitude that words cannot fully capture. Thank you for your endless prayers, unwavering belief in me, and steadfast support that have been the foundation of my achievements. Your love and sacrifices have made all of this possible.

To my little sister, thank you for always being there for me. Your support and encouragement have been a source of comfort and motivation. Your presence in my life has been a constant reminder of the importance of family and unconditional love.

I would also like to extend my heartfelt thanks to my mother, father, and sister-in-law for their love and support. Your encouragement has been a crucial part of my journey, and I am deeply appreciative of your unwavering faith in me.

Lastly, to my dear husband, Yahya, thank you for your continuous support and unwavering love. Your belief in my dreams and your constant encouragement have been my anchor throughout this journey. You have been my rock, providing me with strength and inspiration, and I am deeply grateful for your presence in my life.

This accomplishment would not have been possible without each and every one of you. Thank you for being a part of this journey with me.

ABSTRACT

The popularity of additive manufacturing has been growing over the last few decades. Additive manufactured composites have a wide range of applications in engineering sectors specifically in aerospace structures. In addition to mechanical loads, they are subjected to thermal loads caused by aerodynamic heating. Temperature increases cause changes in material properties, which complicates thermal stress analysis. This PhD work aims to analyze the influences of various thermal treatments on the mechanical properties, thermal stability, and morphological characteristics of continuous carbon fiber reinforced polymer (CFRP) composites printed using the modified FDM printer. The printed samples were exposed to various thermal modes (prolonged and cyclic) and magnitudes (above- and sub-zero degrees) then were investigated using scanning electron microscope, static tensile testing, and differential scanning calorimetry. It is revealed that the Young's modulus and tensile strength of samples were all degraded after thermal treatment under prolonged temperatures and cyclic temperatures. The samples exposed to thermal cycling at above-zero degrees exhibit higher values of glass transition temperature compared to those subjected to prolonged temperature. Observing the morphological structure on the surface visually revealed a subtle change in the surface morphology before and after thermal treatment at temperatures above zero degrees Celsius. The higher the temperature exposure for both cyclic and prolonged temperature groups at above-zero degrees, the more the damage in the polymer parts. Hence, it is possible to characterize the thermal, morphological, and mechanical properties of CFRP composites printed by modified FDM printer using NDT and destructive methods. The thermal loading was simulated with specific boundary conditions similar to the experiments where the sample was placed inside the oven chamber. While for the mechanical (tensile) testing loading, the sample's geometry was created with gripping lines to be in accordance with ASTM D3039 standards for tensile tests used in experimental work and surface traction for the applied load. The highest modulus and strength were achieved from the intact sample while the lowest mechanical modulus and strength were obtained in the sample with heat treatment at the prolonged temperature of 145°C. At high temperatures, matrices soften affecting matrix-dominated properties such as transverse and in-plane shear stiffness and strength. A good correlation between the predictive models and experimental results is obtained. Hence, it is

possible to determine the degradation processes of AM CFRP using the combination of experimental and numerical approach.

PUBLICATIONS

Journal papers

1. **Isyna Izzal Muna**, and Magdalena Mieloszyk. "Temperature influence on additive manufactured carbon fiber reinforced polymer composites." Materials 14.21 (2021): 6413.

2. **Isyna Izzal Muna**, Magdalena Mieloszyk, Ruta Rimasauskiene, Nabeel Maqsood, and Marius Rimasauskas. "Thermal effects on mechanical strength of additive manufactured CFRP composites at stable and cyclic temperature." Polymers 14.21 (2022): 4680.

3. **Isyna Izzal Muna**, and Magdalena Mieloszyk. "Thermal and morphological studies of additively manufactured CFRP composites under thermal loadings." Journal of Transactions of The Institute of Fluid Flow Machinery 142 (2023): 3-12.

4. Maqsood, Nabeel, Swarup Mahato, Marius Rimašauskas, and **Isyna Izzal Muna**. "Experimental analysis, analytical approach and numerical simulation to estimate the elastic modulus of 3D printed CCFRPC under mechanical loadings." Journal of the Brazilian Society of Mechanical Sciences and Engineering 45.9 (2023): 456.

5. **Isyna Izzal Muna**, and Magdalena Mieloszyk. "Numerical modeling of thermal effects on the mechanical behavior of additive manufactured continuous carbon fiber reinforced polymer: From microscale to macroscale." Procedia Structural Integrity 54 (2024): 437-445.

6. **Isyna Izzal Muna**, and Szymon Winczewski. "Molecular Dynamics simulations of thermal conductivity of penta-graphene." TASK Quarterly 24 (2020): 191-220.

Conference papers

1. **Isyna Izzal Muna**, Ruta Rimasauskiene, and Magdalena Mieloszyk. "Numerical modeling of thermal effects on the mechanical behavior of additive manufactured carbon fiber reinforced polymer." Health Monitoring of Structural and Biological Systems XVII. Vol. 12488. SPIE, 2023.

2. **Isyna Izzal Muna**, and Magdalena Mieloszyk. "The numerical model of additive manufactured carbon fiber reinforced polymer under mechanical loading." Nondestructive Characterization and Monitoring of Advanced Materials, Aerospace, Civil Infrastructure, and Transportation XVI. Vol. 12047. SPIE, 2022.

3. Mieloszyk, Magdalena, Katarzyna Majewska, Artur Andrearczyk, **Isyna Izzal Muna**, Ruta Rimasauskiene, and Marius Rimasauskas. "Sub-zero temperature influence on the durability of additive manufactured composite with embedded fiber Bragg grating sensors." Health Monitoring of Structural and Biological Systems XVII. Vol. 12488. SPIE, 2023.

Scientific monographs

1. **Isyna Izzal Muna**, Introduction to Thermal Degradation on Additive Manufactured Polymeric Composites, chapter in: Wybrane zagadnienia inzynierii mechanicznej 2021, Praca zbiorowa pod redakcja M. Mieloszyk, T. Ochrymiuka, Wydawnictwo Instytutu Maszyn Przeplywowych PAN, Gdansk, 2021, ISBN 978-83- 66928-00-8.

"I was born not knowing and have had only a little time
to change that here and there."

- Richard P. Feynman

TABLE OF CONTENTS

List of Figures

List of Tables

Abbreviations

ABS	acrylonitrile butadiene styrene
AM	additive manufacturing
CAD	computer aided design
CCF	continuous carbon fiber
CFRP	carbon fiber reinforced polymer
CLT	composite laminate theory
DSC	differential scanning calorimetry
FDM	fused deposition modeling
FEM	finite element method
PLA	polylactic acid
ROM	rule of mixture
MD	multidirectional
NDT	non-destructive testing
SEM	scanning electron microscope
SCF	short carbon fiber
Tg	glass transition temperature
Tcc	cold crystallization temperature
Tm	melting temperature
UD	unidirectional

Chapter 1

Introduction

The presented work in this dissertation is an outcome of a 4-year project, Thermal degradation processes of additive manufactured structures, funded by the Polish National Science Center under grant agreement no. 2019/35/O/ST8/00757, and the the Foreign doctoral fellowship program, funded by Polish National Agency for Academic Exchange under grant no. PPN/STA/2021/1/00006. Additionally, I would like to acknowledge Centrum Informatyczne (CI) TASK, Gdansk, for allowing me to perform calculations in ABAQUS.

1.1 Problem statement

Additive Manufacturing (AM), also known as 3D printing has been very popular for decades in fabricating a wide range of techniques used to fabricate different 3D shapes. Nowadays, there is a numerous 3D printer system manufacturers available in the marketplace across the world which is developing up to 170 and some well-known products are includes: 3D-Systems, Stratasys, Fusion3, Formlabs, Desktop, Metal, Prusa, and Voxel8, among many others. In 3D printing process, generally a wide range of complex structures and geometries are produced by depositing and stacking filament materials layer upon layer to the substrate platform from a digital data model using Computer Aided Design (CAD) software. This AM process is in contrast to the subtractive method in which the material is conventionally removed from a bulk during the manufacturing process to generate sample parts. The development of high-performance polymers, metals, ceramics, and composites compatible with AM processes has expanded the range of applications, including aerospace, automotive, healthcare, and consumer goods. Carbon fiber reinforced polymer (CFRP) composites have garnered significant attention due to their excellent mechanical properties, including high

strength-to-weight ratio and corrosion resistance. AM techniques have further revolutionized the production of CFRPs which offer enhanced design flexibility and the potential for complex geometries, lightweight, high-performance components. The ability to customize the fiber orientation and distribution in CFRP composites during printing offers unparalleled design flexibility and performance optimization. However, the performance of AM CFRPs in real-world applications (e.g. aerospace and bridge engineering) is influenced by various factors, including exposure to extreme temperature fluctuations both above and below ambient conditions. At extreme above temperatures, AM CFRPs composites undergo thermal degradation processes that can compromise their mechanical properties and structural integrity. Elevated temperatures can lead to the degradation of the polymer matrix, resulting in reduced stiffness, strength, and dimensional stability of the composite material. Additionally, exposure to high temperatures can accelerate chemical reactions within the polymer matrix, leading to degradation, oxidation, and ultimately, material failure. Understanding the thermal degradation mechanisms at extreme above temperatures is essential for predicting the performance and lifespan of additively manufactured CFRPs in applications such as aerospace, automotive, and industrial components. Conversely, at subzero temperatures, AM CFRPs experience challenges related to thermal contraction and brittleness. Low temperatures can cause the polymer matrix to become rigid, leading to increased brittleness and reduced impact resistance of the composite material. Additionally, thermal contraction of the CFRP components can result in dimensional changes and internal stresses, which may lead to cracking or delamination. Understanding the effects of subzero temperatures on the mechanical behavior and durability of additively manufactured CFRPs is critical for applications in cold environments, such as polar research stations, aerospace components exposed to high-altitude conditions, and automotive components in winter driving conditions.

In aerospace applications, AM CFRPs are utilized in various components, including structural elements, engine parts, and interior panels. These components are exposed to extreme temperature conditions during flight, such as the high temperatures generated by jet engines or the cold temperatures experienced at high altitudes. Thermal degradation of additively manufactured CFRPs can impact the structural integrity and performance of aerospace components, posing safety risks for aircraft operations. Therefore, understanding the thermal degradation mechanisms of CFRPs at extreme temperatures is essential for ensuring the reliability and safety of aerospace structures and systems. Moreover, in automotive

engineering, AM CFRPs are increasingly used in lightweight vehicle components to improve fuel efficiency and performance. Automotive components, such as engine parts, chassis components, and body panels, are subjected to a wide range of temperature variations during operation. Thermal degradation of CFRPs can affect the mechanical properties and structural integrity of these components, leading to reduced vehicle performance and reliability. Understanding the thermal degradation behavior of AM CFRPs at extreme temperatures is crucial for optimizing the design and performance of automotive components in diverse operating conditions.

Studying the thermal degradation of CFRP composites fabricated with AM at extreme above and subzero temperatures is essential for understanding their performance limitations and developing strategies to enhance their reliability in diverse applications. Research in this area can lead to the development of advanced CFRP formulations, manufacturing techniques, and predictive models to optimize the design and performance of these materials in extreme environments. Ultimately, this knowledge will contribute to the advancement of aerospace, automotive, and industrial applications, ensuring the safety, reliability, and structural integrity of CFRP components in various operating conditions.

1.2 Purpose of the Study

Understanding the thermal degradation of additively manufactured CFRP composites at extreme temperatures is imperative for advancing various industries reliant on these materials. In aerospace engineering, where CFRPs are extensively used in aircraft components, the ability to withstand extreme temperatures is paramount for ensuring flight safety and reliability. Components such as engine parts and structural elements are subjected to high temperatures during operation, and understanding how CFRPs respond to such conditions is crucial for optimizing their design and performance. Similarly, in automotive engineering, CFRPs are increasingly utilized in lightweight vehicle components to improve fuel efficiency and performance. However, exposure to both high temperatures, such as those in engine compartments, and subzero temperatures, such as those experienced during winter driving conditions, can impact the structural integrity and longevity of CFRPs. Therefore, studying the thermal degradation of these materials at extreme temperatures is essential for enhancing the safety and reliability of composite structures.

Moreover, the renewable energy sector, particularly wind energy, relies on CFRPs

for manufacturing lightweight and durable wind turbine blades. These blades are exposed to a wide range of environmental conditions, including extreme temperatures, high winds, and moisture. Understanding how CFRPs degrade at both above and subzero temperatures is critical for evaluating the long-term durability and performance of wind turbine blades. By studying the thermal degradation mechanisms of CFRPs under such conditions, researchers can develop strategies to mitigate material degradation and enhance the reliability of wind energy systems. Additionally, the transportation infrastructure sector, including bridges and railways, utilizes CFRPs in structural components to reduce weight and improve structural efficiency. However, these components are exposed to temperature extremes throughout their service life, which can lead to thermal expansion, contraction, and ultimately, material degradation. Therefore, investigating the thermal degradation of additively manufactured CFRPs at extreme temperatures is essential for ensuring the safety and longevity of transportation infrastructure.

Furthermore, advancements in AM technology have opened up new opportunities for producing complex CFRP components with tailored properties. However, the performance of AM CFRPs under extreme temperature conditions remains relatively unexplored. Research in this area can lead to the development of novel CFRP formulations and manufacturing techniques optimized for specific temperature ranges and application requirements. Additionally, understanding the thermal degradation behavior of additively manufactured CFRPs can facilitate the development of predictive models and simulation tools for assessing the performance of these materials in extreme environments. Ultimately, studying the thermal degradation of additively manufactured CFRPs at extreme temperatures will not only enhance the safety and reliability of critical infrastructure and transportation systems but also drive innovation in material design and manufacturing processes.

Chapter 2

State of the art

2.1 Literature review

2.1.1 Additive Manufacturing

The concept of additive manufacturing dates back to the 1980s when the first commercial 3D printing technologies were developed for rapid prototyping applications. Initially, these technologies utilized stereolithography (SLA), selective laser sintering (SLS), and fused deposition modeling (FDM) to create prototypes layer by layer. Over time, additive manufacturing evolved with the introduction of new materials, improved printing techniques, and enhanced process capabilities, leading to its widespread adoption across various industries. In recent years, AM has experienced significant growth and innovation, driven by advancements in materials science, printing technologies, and design optimization software. Not long after the discovery of SLA, Carl Deckard filed a patent for the selective laser sintering (SLS) technology. The patent was issued in 1989 to DTM, Inc., a company later acquired by 3D Systems. In 1989, Scott and Lisa Crump file for a patent for fused deposition modeling (FDM). Scott Crump would go on to co-found Stratasys, Inc. While Hans Langer establishes EOS GmbH in Germany and becomes an industry leader in laser sintering research. These remarkable 3D printing innovations were only developed in less than a decade, which has been an incredible time. With the earlier patents expiration, the manufacturers are then able to create new 3D printing devices, making AM technology more available.

The expeditious development in the manufacturing techniques and design of new materials and structures in the engineering sector has sparked a great interest in industry and scientific research. AM also known as rapid prototyping (RP) or three-dimensional (3D) printing is a set of manufacturing techniques that allow producing 3D components with complex geometries in a layer-by-layer manner.

Complex composite structures, which are difficult to fabricate using conventional composite fabrication techniques can be easily manufactured via 3D printing with minimal expense, material waste, and machine setup time. 3D printing has been used to efficiently design the unique auxetic and honeycomb cores [1]. Such structures may overcome the constraints of debonding/delamination of the face sheet from the core during shock/impact effects.

As the most renowned 3D printing process technique, the Fused Deposition Method (FDM) has been adopted by large scale industries for fabricating parts in aerospace, architectural, toy fabrication, and medical fields due to low cost, high speed, flexibility, and simplicity [2]. This process is included as material extrusion which consists of a build platform, print bed, liquefier head and build material spool [3]. Technically, object models are firstly created in the computer-aided design (CAD) software that the STL file format will be obtained. Then, it is imported to the software in which it is sliced into thin two-dimensional contour layers using the tool paths motion [4].

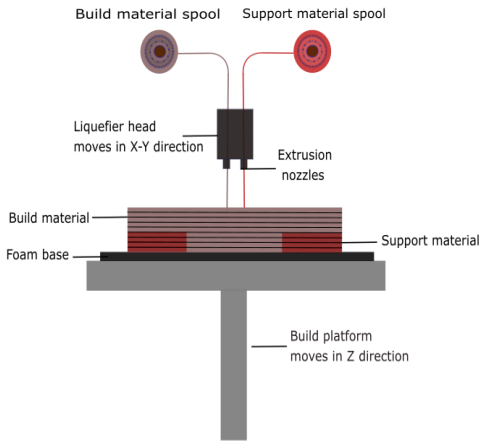

Figure 2.1: Schematic figure of FDM process. Adapted from [5].

As shown in the Figure 2.1, the material in the FDM process is melted into a liquid state in a liquefier head and then selectively deposited through a small heated rastering nozzle that moves using a 3-axis system controls. The nozzle follows the parts in the cross-sectional geometry (x-y plane) and deposits material onto a building platform to produce 3D parts directly from a CAD model [5]. The deposited semi-molten material then cools rapidly, creates solidification, and bonds with the adjacent rasters, whereas a change of phase occurs simultaneously. In the further step, the head moves downward in the z-direction by some amount of set layer thickness, and the next layer is extruded onto the top of the previous

layer. The process of the material deposition of consecutive layers is repeated until the entire part finishes [6]. The FDM method is now widely used in applications such as modelling, prototyping, and manufacturing.

However, researchers across the world have investigated various physical factors during the FDM printing process affecting the quality of printed materials. The material integrity and properties depend highly on bonding phenomena and bond quality. The bond formation between two layers includes surface contacting, neck growth, and molecular diffusion. The phenomena of weak bonding between beads (intralayer) and layers (interlayer) led to the voids formation, dimensional imprecision, surface roughness, and anisotropy of final printed parts at microscopic scale [3, 7, 8]. The formed voids resulting in the low strength of the FDM parts compared to the parts made by other processes such as injection molding [3]. Additionally, many scientific works for the FDM finished material parts have also been explored to study their quality, part integrity, and properties which immensely depend on its bonding quality [3, 9–11].

These issues are highly depending on the parameters of the printing process that can be categorized as follow [3]:

(a) Material parameters.

- Polymer type: For printing amorphous polymers, the FDM technique is highly suitable because they can solidify faster with less degree of shrinkage which is essential to stick to the upcoming layer. However, the solidification of semicrystalline polymers may take longer time depending on the cooling rate and the degree of crystallinity. The crystalline nature also causes a high degree of shrinkage and part distortion.
- Filler type: discontinuous (particles, short fibers) and continuous fibers.
- Filler morphology: size and shape of discontinuous reinforcement.

(b) Printing machine parameters.

- Build orientation: It refers to the inclination of the part in a build platform with respect to X, Y, Z axis. X and Y-axis are considered parallel to build platform and Z-axis is along the direction of part build.
- Raster angle: Direction of the raster relative to the X-axis of build table
- Layer thickness: It refers to the thickness of the deposited layer.
- Nozzle diameter: It depends upon the type of nozzle used. Commercial printers mostly use 0.4 mm nozzle diameter. During the printing of short fiber or particle reinforced composites, the agglomeration of

reinforcements yields nozzle blockage. For composite material printing, generally high nozzle diameters are recommended.

- Raster width: Width of raster pattern used to fill interior regions of the part
- Number of contours: The number of contours of the part outside.
- Raster to raster gap (air gap): It is the gap between two adjacent rasters in a same layer. Negative air gap refers to the overlap of rasters. Positive air gap allows space between rasters. Printing with zero air gap is highly recommended.
- Infill density: The amount of material that is used to build the part inside. For example; the inner layers of the part can be printed in hexagonal or rectangular pattern.

The major amount of materials used in 3D printing industry are of polymer materials compared to other materials such as metals, ceramics, and concrete due to their diversity, light weight, and ease of adoption to different 3D printing processes [12]. As matrix materials, there two main categories for polymers namely, thermoset and thermoplastic polymers. The distinction of them lie on their reacting behaviour when the heat is applied. In thermoset, the material is strengthen when heated but after the initial forming it cannot be remolded or heated back. In thermoplastics, the material can be reheated, remolded, and cooled as necessary without causing any chemical changes. Thermoplastics typically exhibit excellent toughness, high damage tolerance, good mechanical properties, and excellent shelf life. However, chemical resistance is lower, susceptibility to creep deformation is increased, and resin costs are higher than for thermosets [13]. A common type of polymers available to be employed in FDM process is thermoplastic polymers such as polylactic acid (PLA), acrylonitrile butadiene styrene (ABS), poly-carbonate (PC), nylon, etc. However, since common commercial polymers for 3D printing do not meet the necessary outputs, renewable polymeric materials with good physical properties are a major concern for FDM [2].

Another factor of why polymers are commonly used during printing process is due to its low melting point which enable them to be melted effortlessly as filament for extrusion process in FDM. Nevertheless, the final printed parts possess a distortion caused by thermal expansion of thermoplastic materials which expand in volume during the printing process [7]. Transverse or longitudinal shrinkage, bucking, twisting, or angular distortion are all of type of distortions. Shape distortion can be minimised with the use of a slower printing speed, optimum

nozzle temperature, a 45 ° angle and higher layer thickness [14]. Further, when the final products exposed to the room temperature after printing process, the difference in temperature causes shrinkage in the finished components. Due to shrinkage, the residual stresses are possibly induced in the printed parts which results in non-uniform and unpredictable mechanical properties [15].

The weak management of volatiles caused by polymer condensation reactions can lead to voids of the composite which can degrade the mechanical properties of the material [13]. Therefore, although FDM-based polymer products could have geometric complexity, the lack of mechanical strength and functionality are still limited. So far, neat polymer printed parts are employed only for conceptual prototypes [2]. In all research work of AM area, a promising way to overcome these problems is by combining various materials for achieving desired mechanical and functional properties [7, 15]. In particular, in order to minimize and prevent shrinkage, Huang et.al developed a library focused on the print form that can predict shrinkage of final products and change the drawing accordingly [16].

2.1.2 Materials printed with additive manufacturing

A growing advancement of composite materials that are compatible with current printers has sparked considerable interest. For the matrix, typically the materials used are ceramics, metals, and polymers. Among these materials, polymers are the most common used materials as matrix agent [17]. Employing different reinforcement types to the polymer matrix could enhance the strength of the FDM printed materials. Several types of reinforcement for polymer materials are available in the FDM method such as particle, short and continuous carbon fiber, nanocomposites, glass, and kevlar. Generally, fibers are widely applied in composite applications due to their ability to improve the material properties of the composite. Continuous carbon fibers have the high aspect ratio between length and diameter, which can provide effective shear stress transfer between the matrix and the fiber. Furthermore, it is possible to employ fibers in the AM process with different techniques of the composite part in complex shapes. The fiber reinforcement types are illustrated in Figure 2.2.

At a lamina level (single-ply composite), the arrangement type of continuous fiber around the matrix can be classified as unidirectional fiber and woven fiber (bi-direction, three-dimensional). The elasticity and strength properties of a unidirectional (UD) lamina can be determined at a constituent level (matrix and fiber). In this case, it is essential to describe the micro-structure, including the

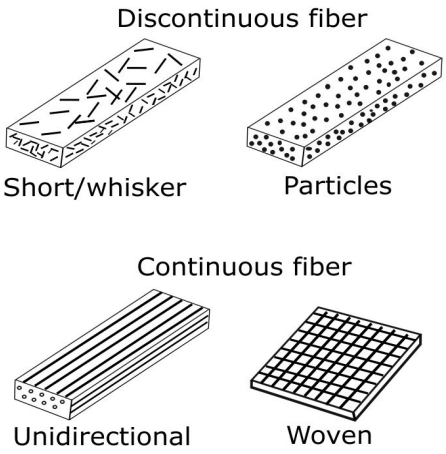

Figure 2.2: Types of fiber reinforcement.

fiber shape and geometrical distribution, and the material properties of the constituents. When the laminate is only unidirectional, it means that the layers are stacked with the same orientation, then the laminate composite can be considered as a single lamina of orthotropic material [18]. The continuous-fibers of the individual layers, plies, or laminae are normally oriented in directions that will enhance the strength in the primary load direction. Unidirectional 0° laminates are extremely strong and stiff in the 0° direction. However, they are very weak in the 90° direction because the load must be carried by the much weaker polymeric matrix [19].

The longitudinal tension and compression loads are carried by the fibers, while the matrix distributes the loads between the fibers in tension and stabilizes the fibers and prevents them from buckling in compression. The matrix is also the primary load carrier for inter-laminar shear (i.e., shear between the layers) and transverse 90° tension. In most cases, stress and strains need to be calculated for every lamina in the laminate. Then, the laminate stacking sequence (LSS) must be calculated. In this case, the elastic properties of each lamina, as well as the thickness and fiber orientation of every lamina, must be given.

Despite the fact that polymer composites have better mechanical properties than pure polymers, composite printed parts through the FDM method still does have inferior properties [3, 14]. These lack of properties exist due to weak interface between matrix and reinforcement of continuous fiber reinforced composites, as well as poor interface stress transfer of particle or short fiber reinforced composites [3]. The quality of printed parts depends on many process variables and it can be controlled by altering printing parameters, such as layer thickness of deposed layer, printing orientation, raster width, raster angle and air gap [7, 12].

In this section, the recent development of printable polymer-matrix composites reinforced by short fibers, continuous fibers, or nanomaterials will be briefly described. Its primary concern is the quality of printed parts through FDM such as void content, anisotropy, and interface strength of the parts [3].

Short carbon fiber-reinforced polymer (SCFRP) composites

Carbon-based fiber (CF) reinforcement has been tremendously studied using FDM printing technique due to its ability to align fiber orientation which could improve the mechanical properties of polymers. Short fiber-reinforced composite fabrics are made of short fibers that are aligned and distributed throughout a polymer matrix. Several research works have been done by scientist by employing short CF into various polymer matrix. Ning et al. reinforced short CF of 7.2 μm diameter and 100 μm length in the ABS using FDM printing [20]. The result showed an improvement of tensile strength and elastic modulus in the printed parts was at 5% and 7.5%, respectively. It is also reported that the increase in the length of carbon fibers increases the strength and modulus but decreases the toughness and the ductility. In a similar study by Tekinalp et al., ABS polymer was reinforced with the short CF of 0.35 mm length which resulted in an increase of 115% in tensile strength and 700% in elastic modulus of the printed parts [21]. With the added short fibers, the voids within the beads exist due to the poor interface between ABS and CF.

An anisotropy of ABS and short CF printed composite was observed by Love et al. It was shown that the tensile properties of specimen printed along longitudinal direction are higher than the properties of the specimen built vertically. Furthermore, the inclusion of short carbon fibers improves thermal conductivity and thermal expansion coefficient, both of which are important for the printed parts' dimensional stability [22]. Different polymer matrix material was used by Ferreira et al. to observe the strength of FDM printed parts. PLA (polylactid) was used and reinforced with chopped short CF of 60 μm length. It is demonstrated that in comparison with neat PLA printed parts, the tensile and shear modulus of the reinforced composites are higher than about 100 %. It has also been observed that the fibers are aligned along the filament's length during extrusion and are aligned along the print direction during printing [23].

Continuous carbon fiber-reinforced polymer (CCFRP) composites

Continuous carbon fiber-reinforced polymer (CCFRP) is highly applied in the engineering field among any other type of reinforcement material, owing to its improved tensile strength, lightweight, greater stiffness, and low thermal expan-

sion. [24, 25]. Many extensive studies have been conducted to investigate the strength of printed continuous CFRP composite using FDM technique [24, 26–30]. Tian et.al. proposed CCFRP materials by employing continuous CF and PLA filament which were being stacked into the FDM 3D printing process simultaneously. During the forming process, the influence of process parameters such as temperature and pressure are important to study the interfaces and performance of printed composites. Interface and carbon fiber content are technical factors for the composites specifications. It was found that flexural strength of 335 MPa and modulus of 30 GPa were obtained when the fiber content reached 27 % [28].

In similar work, Matsuzaki et al. developed a method for 3D printing of CCFRP based on FDM using continuous carbon fiber tows and jute twisted yarns as reinforcements in PLA as the matrix which enables direct 3D fabrication without the use of molds. It was shown that the tensile strength and modulus of CCFRP composite printed parts are higher than values shown by conventional composite printing techniques. It is also reported that the mechanical properties of these parts can be further improved by increasing the volume fraction of continuous fibers [24]. Akhoundi et al. conducted experimental investigation with maximizing the fiber content in order to improve the mechanical strength of FDM based continuous CF-PLA composites. It was reported that around 50% fiber-volume content is achieved and the tensile strength and modulus are of 478 MPa and 29.4 GPa, respectively [26].

In a separate study, the process of directly introducing fiber reinforcement into the thermoplastic filament while printing was discussed [27]. The process involves embedding a 7 μm diameter CF filament continuously into the melted polymer filament just before the deposition of the layers. The tensile modulus of the printed part showed more than 200% improvement while the bending modulus improved around 370%. The failure strain of the composite was less than that of pure PLA. Another study has been carried out by Nabeel et.al compared the mechanical characterization of four different samples: neat PLA, PLA reinforced SCF, PLA reinforced CCF, and PLA reinforced SCF-CCF [31]. The result shown that, PLA-CCF specimens have the highest tensile strength of 245.4 MPa and Young's modulus of 27.93 GPa compared to other samples. It was also proved that the Young's modulus could be improved and decreasing ductility by increasing the fiber's content.

Goh et al. processed continuous carbon and glass fiber composites using FDM

[29]. Nylon matrix pre-impregnated fiber filaments are used as feed stock. The failure mechanisms in each mode were investigated in this analysis, which included tensile, flexural, and indentation tests. The main failure mechanisms in these tests were found to be tensile rupture perpendicular to loading direction, shear damage along the fiber direction, debonding between adjacent filaments, and delamination. Dickson et al. used two separate print heads to print continuous CF reinforced composites, with nylon printed in one stage and reinforcement printed in the other [30]. It is reported that the isotropic pattern yields excellent properties in tension and the concentric pattern yields better properties in bending behaviour.

Furthermore, it has been stated that increasing the fiber volume fraction increases the strength of continuous fiber reinforced composites. For example, the tensile strength of 33 % glass fibers printed in a concentric pattern, is comparable to aerospace grade aluminum [30]. However, as the sum of fiber increases, the void proportion often increases limiting the maximum fraction of fiber length. Li et al. investigated the mechanical properties of modified continuous CF-reinforced PLA composites fabricated using an FDM printer [32]. In this experimental study, the result indicated that the tensile strength and flexural strengths of modified carbon fiber reinforced composites were 13.8% and 164% higher than original carbon fiber reinforced samples. It was shown through scanning electron microscope (SEM) results that a better fiber-matrix bonding interface of the carbon fiber was achieved.

Nanocomposites

Some other investigations have also been carried out to find the effect of other carbon derivatives such as carbon nanotubes and graphene on PLA. Nanomaterials can be introduced in a 3D printed part either manually or automatically with intermittent stoppages or through premixing into the host matrix [2]. When nanomaterials are incorporated and blended into host matrices through 3D printing, there is significant potential for nanocomposite development. As a result, improving nanocomposites output in terms of consistency and durability, cost, and thermal instability may provide advantages and new opportunities [2].

Zhang et al. processed FDM parts using carbon nanotube (CNT) reinforced ABS and carbon fiber reinforced ABS composites [33]. It was discovered that the strength and modulus of printed parts are higher for these two composite material systems, despite the fact that the void content in the printed parts is higher compared to pure ABS printed parts. Carbon nanotube reinforced ABS

printed parts showed less void content than carbon fiber reinforced ABS printed parts. Printing at a lower layer thickness of 0.8 mm, a slower printing speed of 60 mm/s, and 0 degree raster orientation yielded the best results.

In similar research by Shofner et al., CNTs were also used as an additive in ABS polymer fabricated with FDM technique [34]. It was reported that FDM components filled by CNTs increased by 5 wt % to 31 % tensile strength, but their strain decreased significantly. Another interesting study has been presented by Sweeney et al. to increase the interlayer strength by heating polymer interfaces locally [35]. Before printing, the PLA filament is coated with CNTs. During the printing process, localized heating at the nanoscale with microwaves causes the surfaces to melt and facilitates inter layer adhesion. The study found that local welding by microwave heating increased fracture strength by 275%. Boparai et al. have tested the possibility to use a 3D printing technology Nylon 6 based nanocomposite rather than ABS polymer [36]. The particles were observed using Scanning Electron Microscope (SEM) to be uniformly dispersed and as an alternative to ABS matrix the Nylon-6 can be used.

2.1.3 Damage detection of additive manufactured materials

Additive manufacturing (AM) materials is still developing for further improvements in order to make their functionality optimal and to prevent the fatal failures. The ability of early detection of thermal damage and failures on AM samples is of importance to develop the appropriate characterization methods for polymer composites. In previous section, different forms of damage on composite structures have been discussed. There are several similar approaches used in the damage detection includes Nondestructive Testing (NDT) also known as Nondestructive Evaluation (NDE), Structural Health Monitoring (SHM), Condition Monitoring (CM), Health and Usage Monitoring System (HUMS), Statistical Process Control (SPC) and Damage Prognosis (DP) [37]. This section will briefly describe the damage inspection in NDT and SHM as well as the distinction between them.

Nondestructive testing (NDT) Nondestructive Testing (NDT) method is used to detect the damage assessment in different life stages of a composite material. These stages are: First, to predict its performance under load in conjunction with impact/fatigue testing; Next is before the assembly, to ensure the material is free of manufacturing flaws; and, finally, to identify in-service degradation. Certain the sensitivity to impact events, the impact damage resistance is evaluated using

particular tests designed to detect the energy that induces delamination of a given extension [38].

The methods used for conventional NDT include ultrasonic inspection, optical inspection, eddy current, acoustic emission, thermography, radiography, vibration analysis, and lamb-waves. Thermography and ultrasonic testing are the most suitable standardized NDT techniques allowing detecting different types of damages. Thermography and ultrasonic testing are the most suitable standardized NDT techniques allowing detecting different types of damages. Although ultrasonic is broadly used technique for defect detection in composites, it is considered as not simple inspection due to their anisotropy and complex structure [38]. The propagation of ultrasonic waves in additively manufactured parts will be affected by defects, so it can reflect defect information in parts. NDT is mainly used to detect defects such as pores and cracks [39].

Eddy current (EC) method is a type of NDT that uses the principle of electromagnetic induction to identify defects in conductive materials by measuring changes in induced eddy currents. Eddy current testing technology can be used in harsh environments since it satisfies some of the AM requirements for NDT and is suitable for detecting defects such as cracks and non-fusion pores [39]. Radiography is a non-destructive technique for determining the presence of defects and the internal state of structures. Radiography includes the projection and penetration of radiation energy onto and through the substance being investigated. Except in locations where thickness or density variations occur, the radiation energy is absorbed uniformly by the medium [39].

Acoustic emission (AE) and infrared thermography (IRT) have been combined simultaneously to identify damage evolution in carbon fibre reinforced composites by Munoz et al [40]. With acoustic emission technique, the energy released during a damage process is detected by piezoelectric sensors in form of transient elastic waves. It was determined that there is a correlation threshold below which the two types of damage cannot be associated and over which they can be caught by both methodologies. Furthermore, the study confirms the complementary of AE and IT and identifies the special sensibility of each method in relation to each mechanism [40].

Due to technical advancements, non-destructive testing (NDT) may now be conducted throughout the manufacturing process. NDT is used during manufacturing, such as additive manufacturing (AM), to ensure that possible defects are made out rather than needing to be fixed afterwards; the component is subjected

to NDT to check that the manufacturing process was successful. Once the component is in service, it may be subjected to further NDT throughout its life [41].

Structural health monitoring (SHM) Various SHM methods have been developed for a wide range of applications, including bridges, offshore structures, and aerospace structures. Each of the established SHM methods is created with the unique needs of the application in mind [42]. The present state of the art in the field of SHM is capable of detecting and locating damage. The following are the most widely utilized SHM methods in various structures:

(a) Vibration monitoring;

(b) Strain monitoring;

(c) Wave propagation–based monitoring

The techniques listed above have been developed for more than a decade and there are several variants of each of the techniques developed based on the processing or the feature extraction.

Vibration monitoring

One of the early SHM approaches established was vibration monitoring. Natural frequencies, mode forms, mode shape derivatives, damping qualities, and other procedures and monitored quantities are among the techniques and monitored quantities in vibration-based SHM [42]. A typical SHM approach is active vibration-based technology. The method's core premise is that structural dynamic characteristics are functions of physical variables including mass, stiffness, and damping. As a result, physical property changes can result in observable variations in vibration responses. Frequency, mode shape, power spectrum, mode curvature, frequency response function (FRF), mode flexibility matrix, energy transfer rate (ETR), and other dynamic characteristic parameters are frequently employed in the approach [43].

Strain monitoring

A strain-based-SHM approach is a method that uses only strains as input data to detect and localize early anomalies in a structure in service. In the healthy structure, the strains supplied in each location are correlated with the strains measured in the area using neural networks that establish rules between strains with the goal of fixing the reference structure's fingerprint. Any potential change in the structure from its reference state is identified and localized as a result of a change in the laws of the correlation between the strains at a particular place. To measure strains, optical fibers may be installed with attached on the surface

of the structure that can offer a distributed strain measure via the distributed Bragg reflector [44].

A study researched smart 3D structures with embedded and printed sensory elements. The embedded strain sensor was based on the conductive Polylactic acid (PLA) material. The research was focused on dynamic measurements of the strain and considered the theoretical background of the piezo-resistivity of conductive PLA materials, the temperature effects, the non-linearities, the dynamic range, the electromagnetic sensitivity and the frequency range. A quasi-static calibration used in the dynamic measurements was proposed. It was shown that the temperature effects were negligible, the sensory element was linear as long as the structure had a linear response, the dynamic range started at approximately 30 $\mu\epsilon$ and broadband performance was in the range of few kHz (depending on the size of the printed sensor). The promising results support future applications of smart 3D-printed systems with embedded sensory elements being used for dynamic measurements in areas where currently piezo crystal-based sensors are used [45].

Wave propagation-based monitoring

The wave propagation–based monitoring techniques developed by SHM include acoustic emission (AE)-based techniques as well as elastic wave–based approaches such as guided waves (GW). The various advantages of GW are : (1) A short wavelength allows for plenty of interaction between GWs and relatively small defects; (2) These waves have a very high excitation frequency, so low-frequency ambient influence can be filtered out; (3) These waves can propagate for a long distance inside the structure under investigation; and (4) It provides better sensitivity to various types of defects and the extent of the monitoring [46]

An SHM system consists of hardware (sensors, actuators, and related instrument) and software elements for detecting damage, modeling, and analyzing the impact of damage on the mechanical behavior of composite structures [47]. An actuator is utilized to generate the waves in these procedures. Transducers receive signals at one or more locations, which are then analyzed for defect identification. Contact transducer of many sorts, typically consisting of an electroactive and magnetoactive material for excitation and detection of acoustic waves is possible. These materials are capable of changing their properties when triggered by an electric or magnetic signature and react by stress/sensor [48]. The sensors and transducers used in GW based SHM that can be adapted for the inspection in composite structures are:

- Piezoelectric sensors
- Fiber optics
- Microelectromechanical systems
- Scanning Laser Doppler Vibrometer

To summarize, while NDT is employed during the manufacturing process to foresee the possible defects rather than to investigate it afterwards, SHM uses the information gathered at the manufacturing stage, where manufacturing flaws that were within tolerance were located using NDT [41]. SHM refers to the wide idea of continuous, in-service assessment of structures utilizing a number of inspection techniques. The heart of the technology is the creation of autonomous sensor systems for the continuous inspection of structures with low manpower requirements. Not only is structural failure detected but physical harm also early indication, so that repair solutions are identified before a failure leads to structural damage [49]. In the above concept, SHM is the overall aim, using NDT for initial evaluation and additional testing when required.

Other detection techniques

In the previous subsections, the techniques mentioned were used for detecting the physical damages of AM materials. However, further inspection in material characterisation is also crucial for fully realising the advantages of AM. Spectroscopy is a set of techniques used in order to determine how electrons respond to light energy. Its characterisation procedures provide chemical analysis regimes that aid in the identification of materials and the determination of elemental composition. This data may then be utilized to confirm material stability following processing, the existence of functional components inside produced parts, and the purity of raw materials. As a result, spectroscopic characterization can be beneficial for quality and process control [50]. The basic principle of all techniques is shining a beam of electromagnetic radiation onto a sample and observing how it responds to such a stimulus. Primarily, upon interaction with the sample, the radiation is either absorbed, reflected or scattered is some manner. The response is recorded as a function of radiation wavelength, resulting in a response plot (spectrum) [50]. Several spectroscopic techniques, including laser confocal microscopy, Fourier transform infrared (FTIR) spectroscopy and photoacousitc FTIR spectroscopy, Raman spectroscopy, and X-ray photoelectron spectroscopy (XPS) in order to characterize both the bulk and surface chemistry of the source material and printed samples. Several microscope techniques such as optical microscopy, scanning electron microscopy (SEM), and atomic force micrsocope (AFM) are

also commonly used methods for damage characterization. The primary goal of microscopy is used to visualize objects with respect to the size of materials.

2.1.4 Material degradation of additive manufactured composites

In section 1.4. it has been briefly described that there are several drawbacks (e.g. defects) in FDM printed polymer composites which are affected by printing process and different printing parameters. Some of these defects are shrinkage, distortion, and voids formation issue [7, 13, 15]. Previously, in section 1.5. the degradation term and thermal degradation process on polymer composite has been explained. The damage caused by at least one of subjected temperature conditions such as continuous exposure to high temperature, cyclic temperature, and local-global temperature on polymer composite material is referred to as thermal damage. Beside the defects of the AM printed materials, thermal damage is also inevitable. Heat damage occurs as a result of an irreversible thermodynamic shift that results in a physical and/or chemical changes. As several studies have shown that various temperature conditions can cause two types of material damage and this section will briefly discuss the correlation between them [39, 51–53]. The two types of material damage are as follow:

- Physical damage : mass loss, properties degradation, shrinkage, cracking, warpage, blisters, and delamination.
- Chemical damage : depolymerisation, debonding, chain-scission, etc.

Properties degradation

The glass transition temperature (Tg) of resin/polymer in fiber reinforced polymer composite defines a regime where the high stability of its mechanical and thermal properties is shown. When the structure is subjected to thermal stresses equivalent to or greater than Tg, changes or degradation in mechanical properties can be detected as a result of changes in the matrix, the fibre matrix interface, and, eventually, the fibre characteristics themselves [54]. Before the physical damage occurs, chemical degradation is initially formed which results in depolymerisation, random chain scission, side group elimination and carbonisation of the composite. The initial exposure oxidises the matrix, resulting in noticeable surface discoloration as a result of the cross-linking process, which contributes to the emission of volatile gases.

Mass loss

At an extended period of time, charring or mass loss is obtained as a result of

resin pyrolysis and oxygen separate the polymer and eventually destroying it when exposed to high temperatures [51, 53]. Owing to volatilisation of the monomer in chemical degradation, the lose of overall mass is confirmed experimentally via thermogravimetric analysis (TGA). TGA is thermal analysis method where the sample mass is measured over time as the temperature changes. Additionally, mass-loss rates have also been analysed empirically with Arrhenius rate curves. More complex models have coupled modeling of oxygen distribution into the material with chemical reaction rate equations to determine mass loss and the formation of damaged layers [51].

The mass loss in the composite is primarily matrix mass loss, although fibers can also lose mass. In inert atmosphere, mass loss is minimized but not totally eliminated. Mass loss is related with significant shrinking of the material and a decrease in the values of the material's characteristics. Degradation begins at exposed surfaces, where a distinct deteriorated layer can be seen in both neat resin specimens and composites. As time passes, the damaged layer expands. This mechanism is assumed to be governed by the rate of oxygen diffusion into the substance [51]. Additionally, geometry and ply orientation have a major impact on matrix polymer oxidation in carbon-reinforced composites [13]. The analytical method to predict the effects of matrix degradation and shrinkage on the performance of composite laminates had been done by McManus and Chamis [51]. They approached this approach using : (1) existing experimental evidence, an empirical model developed in which shrinkage and changes in properties of the matrix are functions of several different mechanisms for degradation, and (2) the effects of these matrix changes on unidirectional plies are predetermined by fundamental micromechanical principles.

Cracking

Heat, moisture, and oxygen are transferred into the material; the matrix material changes chemically; the changes in the matrix affect the behavior of the composite material at the ply and laminate levels; and this behavior can result in cracking or other failures [51]. Failures such as matrix cracks may then result in much increased admitted oxygen, higher material changes, and more cracking clearly a linked and possibly unstable condition. Eventually, voids and cracks form in the degraded region. Cracks allow oxygen to penetrate deeper into the material, thereby accelerating the degradation process [55]. It was suggested that in extreme cases an interconnected network of microcracks eventually forms, which allows extensive oxidation throughout the laminate and causes the composite to

become completely ineffective. Cracking of these degraded layers can predicted by a finite element model (FEM) that treated the degraded layers as layers with different material properties.

Shrinkage

A resultant shrinkage near the material surface is mainly caused by the thermal exposure at longer time and the material degradation effects on the stress state in polymer matrix composites has been modelled by McManus and Chamis [51]. The ply and laminate behavior due to shrinkage and property changes were predicted using micromechanical and laminate theory relations. Nonuniform shrinkage creates strains, which can lead to ply breaking. Degradation also produces a nonuniform material, making it harder to interpret previous test results. The stress at failure in a longitudinal bending test is not the same as that computed by assuming a uniform material, for example. The fractures also have a substantial influence on the findings of transverse bending tests, making them difficult to utilize statistically [51].

Degradation is a complex and coupled process since the investigation of interactions between two individual resulted damage will be unavoidable and it may result in structural deformation of these composite systems [54]. In the future research works, various temperature conditions will be subjected to the AM printed materials and consequently the thermal damages will be investigated. Thus, in order to prevent the failures of samples it is pivotal to understand the damage characterization and quality of composite structures during and/or after thermal degradation process.

2.2 Objective and Motivation

The objective of the doctoral dissertation is to perform analyses of thermal degradation processes of CFRP composites printed with the AM technique specifically the modified fused deposition modeling (FDM) method printer. By examining the history of additive manufacturing, recent advancements, applications of CFRP composites in AM, and the mechanisms underlying thermal degradation, this research contributes to a better understanding of the challenges and opportunities associated with the utilization of CFRP composites in various temperature conditions.

AM has revolutionized the production of CFRPs by allowing for the creation of intricate structures with precise geometries and customizable properties. CFRPs

are composite materials composed of polymer matrix reinforced with continuous carbon fibers, known for their high strength-to-weight ratio and corrosion resistance. The main advantage of AM is a possibility of manufacturing "ready-to-use" elements with complex shapes and limited amount of waste during the production process, so the technique has been adopted for rapid prototyping allows testing new design concepts.

However, despite the wide applicability of CFRPs, these materials are more likely exposed to various environmental conditions and one of the most affecting factor is temperature. CFRPs are susceptible to material degradation when exposed to extreme temperatures, which can compromise their mechanical properties and structural integrity. The problem of material degradation of AM CFRPs arises in various industries and applications where these materials are utilized. Understanding degradation processes will lead to increase structural reliability of constructions where traditionally manufactured materials are going to be replaced by AM. The differences in material structures between additive and traditional manufacturing elements will lead to possible differences in degradation processes.

The thermal degradation study is investigated using experimental and numerical approaches. The experimental works include additive manufacturing process with the FDM method, mechanical testing, thermal characterization using differential scanning calorimetry (DSC), morphological characterization using non-destructive testing (NDT) techniques such as scanning electron microscopy (SEM) and optical microscopy. The numerical works include numerical simulation using Abaqus software as finite element modeling (FEM) method tool to study the effect of temperature exposure on the mechanical strength of AM printed samples and CLT method using the python script. The doctoral project was realized in the international cooperation between the Institute of Fluid Flow Machinery, Polish Academy of Sciences, IMP PAN, Poland; and Kaunas University of Technology, KTU, Lithuania. In the middle of the project PhD student internship in KTU was performed. During the internship, the manufacturing process of CFRP composites and a part of experimental investigations were performed.

Based on the literature review, the following thesis could be formulated.

Main thesis It is possible to determine the thermal degradation processes of AM CFRP using the combination of experimental and numerical work.

Another aim of this PhD work focuses on characterizing the structural, thermal and mechanical properties of CFRP composites manufactured using the modified

FDM method after being treated under different thermal conditions. Additionally, the mechanical testing results obtained from numerical simulation are compared to the experimental investigation.

Sub-thesis 1: Characterization of the thermal, morphological, and mechanical properties of the CFRP composites printed by modified FDM printer.

The final aim of this research work is the determination of the relationships between thermal loading parameters (e.g. magnitude, exposition time), structural and mechanical changes. The thermal analysis is proposed to aid in understanding the structural nad mechanical behaviour after undergoing thermal treatment such as matrix brittleness and degraded tensile strength.

Sub-thesis 2: Determining the relationships between thermal loading parameters (e.g. magnitude, exposition time) and structural and mechanical changes in CFRP elements manufactured using the modified FDM method.

This research seeks to provide knowledge into the understanding of thermal degradation process in CFRP composites produced with a modified FDM printer as AM method compared to the conventional manufacturing method. The structural, mechanical, and thermal analysis of CFRP composites under thermal exposures will be analyzed.

2.3 Thesis Contribution

This research work is composed of two different tasks:

i. Experimental work: The experimental investigations encompass an additive manufacturing process employing the Fused Deposition Modeling (FDM) technique, mechanical testing, and thermal analysis via Differential Scanning Calorimetry (DSC). Additionally, morphological characterization is conducted using non-destructive testing (NDT) methods, including Terahertz spectroscopy and Scanning Electron Microscopy (SEM).

ii. Numerical work: The numerical analyses incorporate comprehensive simulations utilizing Abaqus software, employing the Finite Element Modeling (FEM) methodology to scrutinize the impact of thermal exposure on the mechanical integrity of additively manufactured specimens. Additionally, the studies extend to include the Classical Lamination Theory (CLT) method, implemented through

custom Python scripting, to further elucidate the behavior and performance of the printed samples under varying thermal conditions.

2.4 Thesis Organization

The PhD thesis is arranged as follows:

- Chapter 2 will present the state of the art in AM of CFRP composites, including AM history and applications. This chapter will introduce various techniques and materials printed with AM methods. Furthermore, an overview of the damage detection of AM materials and the degradation process of AM composites will be presented;
- Chapter 3 will present the experimental method covering the manufacturing process of CFRP composites using the FDM method, thermal treatment of printed samples at various magnitudes of temperature (negative, positive), and exposition time (continuous, elevated, cycle). The characterization of the morphological structure will be investigated to reveal the porosity, defects, and damage within these structures by performing NDT methods. The thermal properties of 3D-printed composite parts will be determined using differential scanning calorimetry (DSC) and tensile testing will be performed to measure the mechanical properties of AM samples.
- Chapter 4 comprises a numerical method to study the influence of thermal treatment on the mechanical strength of 3D printed materials using the finite element modeling (FEM) method and classical laminate theory (CLT). The numerical results then being compared to the experimental results. A detailed analysis of the microstructural defects and fiber orientation induced by the printing processes as well as the related tensile behaviour and damage mechanism is carried out.
- Chapter 5 contains conclusions that consolidate the key findings and results derived from the research conducted throughout the thesis. Building on the conclusions, this section outlines potential avenues for future research. It suggests specific areas where further investigation could be beneficial, highlighting how subsequent studies could build on the current findings to advance knowledge in the field.

Chapter 3

Experimental method

3.1 Additive manufacturing process and materials

3.1.1 Printing process

In this experimental work, unidirectional (UD) CFRP composites were manufactured with the modified FDM printer as experimental specimens at Kaunas University of Technology, Lithuania. The FDM printing equipment MeCreator2 was modified and designed by Rimasauskas et al. [56] before fabricating the test specimens. Pre-impregnation procedure was used for the reinforcement using CCF to improve the printing performance and filament bonding. PLA pellets were dissolved in a 90 g/10 g dichloromethane solution from Euro-chemicals using a magnetically charged LBX H01 mini-stirrer at 600 rpm. The virgin CCF tow (non-impregnated) was run through this polymer and concurrently dried using an air gun at 220°C. The AM process employed impregnated CCF filament and PLA matrix spools which are presented in Figure 3.1.

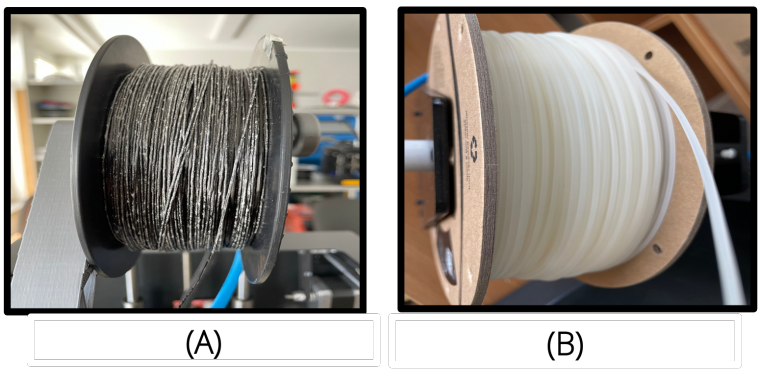

Figure 3.1: Impregnated continuous carbon fiber spool (a); and PolyLactic acid spool (b).

The 3D model of the CFRP specimens was created in a CAD (computer-aided design) package, which was exported as an STL file and subsequently loaded into

a 3D printer slicing software (Simplify3D, Cincinnati, OH, USA). The CAD files of the specimens have been used to deposit the melted thermoplastics from the bottom layer onto the top layer.

The extrusion printing head has been modified with two inputs (one for the fiber component and one for the matrix material) and one output, enabling the material made from polymers to be fused with the fiber throughout the printing process. The impregnated carbon fiber filament was fed directly to the printing nozzle through the printing head. Liquid PLA is joined with impregnated CF and pumped continuously through the printing nozzle while the polymer melts inside the mixing chamber of the heating control unit. The optimal temperature at the printing head for melting the polymer (PLA) and creating a bond with impregnated CCF was 220°C. The PLA material reinforced with carbon fiber is extruded through the printing nozzle on the borosilicate glass printing bed that is mounted on the aluminum plate. It should be mentioned that molten polymer, which is continuously forced via the printing nozzle feeds the CCF tow solely. After printing the composite sample, the cutter will separate the filament spool and the printed part. The borosilicate glass should be removed from the aluminum plate bed to cool before extracting the 3D-printed sample with blades. The modified FDM printer device and configuration of the printed specimen are presented in Figure 3.2. The printing parameters are shown in Table 3.1.

The rectilinear pattern of the printing process is selected, and the extrusion width is 1.4 mm forming nine continuous parallel lines in each deposited layer. The layer height is set to have four layers for each printed specimen, and an extrusion multiplier is used to control the constant amount of filament content. The printing process parameters are shown in Table 3.1.

Table 3.1: Printing parameters

Parameter	**Value**
Nozzle temperature	220°C
Bed temperature	90°C
Interior infill	100%
Infill pattern	rectilinear
Printing speed	3 mm/s
Nozzle diameter	1.5 mm
Extrusion multiplier	0.7
Primary layer height	0.5 mm

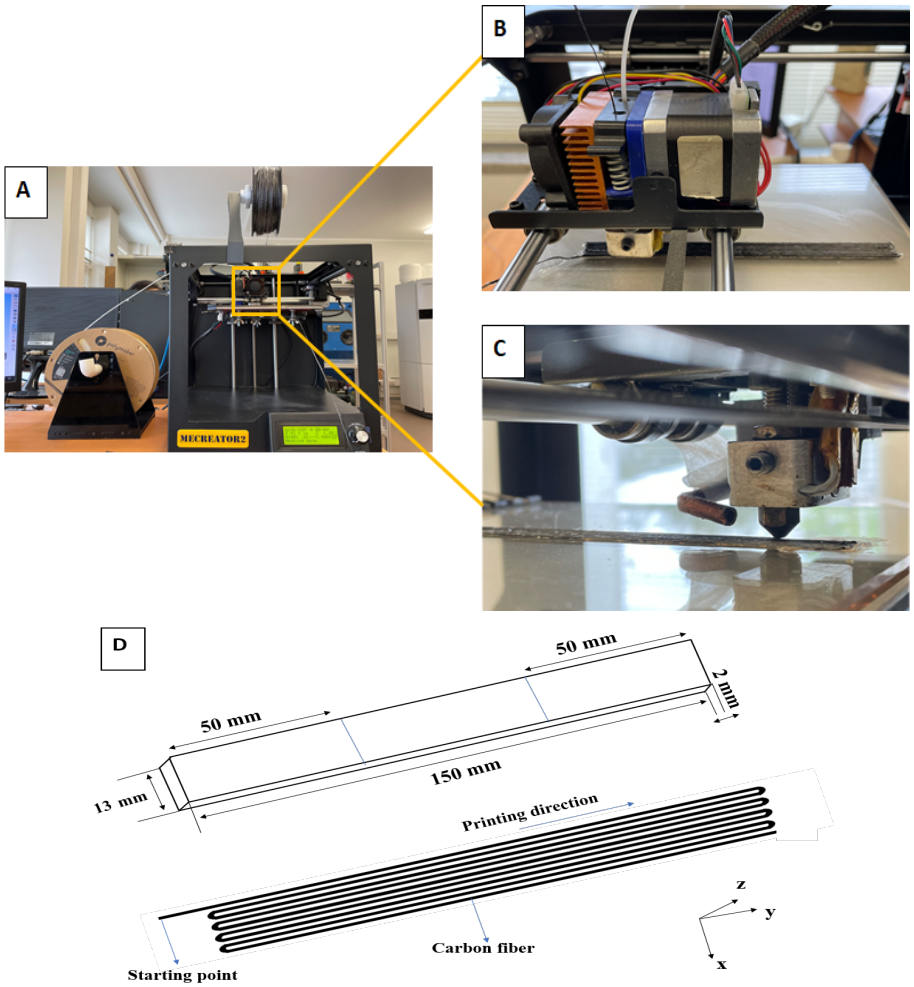

Figure 3.2: Modified FDM printer (A); extruder with two inputs (B); printing nozzle (C); and printed specimen configuration (D).

3.1.2 Materials

The matrix agent used in this experiment was thermoplastic PLA 3D850 filaments (Polymaker), and the continuous carbon fiber (CCF) was T300D-3000 (Toray, France) with 3000 carbon fiber tow. Table 4.1 displays the matrix and fiber agent material properties. Material suppliers provided mechanical property information on all materials. Using CCFs as reinforcement in polymer-based composites has the advantage of keeping the weight light while increasing strength. The mechanical properties of composite materials reinforced with carbon fiber are widely known to be significantly reliant on the carbon content of the material. The approximately carbon fiber content in the matrix was calculated by the tool-path length of the specimen and it can be measured as the weight ratio of carbon fiber to composite specimen [57]. There are nine groups of printed CFRP samples for various thermal treatments as summarized in Table 3.3. In total, the

number of specimens printed was 45 samples in which 5 samples for each group of thermal treatment were required in accordance with the D3039 ASTM standard used for tensile testing. The printed specimens are shown in Figure 3.3. The programmed dimension of the specimen is 150 x 13 x 2 mm and the carbon fiber content of the composite was approximately 18.2%.

Table 3.2: Mechanical properties of composite components

	Elastic modulus (GPa)	Elastic strength (MPa)	Strain at failure (%)	Density (g/cm^3)
Matrix	2.636	46.6	1.9	1.17
Fiber	230	3530	1.5	1.76

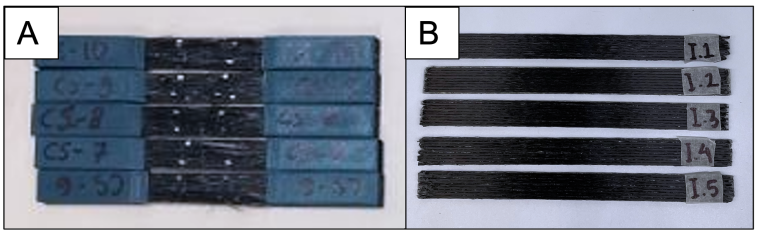

Figure 3.3: Printed specimens with and without gripping tabs used for tensile testing (A) and (B), respectively.

3.2 Thermal loadings on AM CFRP materials

In real environmental life, the printed composite materials are more likely exposed to various environmental conditions, specifically related to temperatures. Composites exposure onto different magnitude, area, and time period will affect its mechanical strength and morphological structure differently. Thermal degradation of additive manufactured polymer composite has not been explored by researchers comprehensively yet it is an important phenomena which will be useful in structural health prediction of light weight material. According to studies, the thermal degradation process is affected by the material, the environment, and the heat source [53]. The damage caused by at least one of subjected temperature conditions such as continuous exposure to high temperature, cyclic temperature, and local-global temperature on polymer composite material is referred to as thermal damage. Over time, an irreversible thermodynamic process caused by heat damage on printed composites will lead to thermal degradation which may result

in structural deformation and/or chemical changes of these composite systems [54]. In attempt to observe thermal damage on printed polymeric composite, many research works have been conducted in defect detection methods using advanced technologies since it is fundamental to observe thermal failures on printed samples as well as its mechanical qualities at early stage [40, 58, 59]. Understanding defects on FDM printed materials and their causes indicate the first step to inspect and eliminate them.

There has been a numerous number of research related to post-processing techniques for reducing defects, enhancing the cross-linking state and crystallinity of molecular chains in AM polymeric composites as well as to improve the mechanical properties of manufactured specimens [60–65]. This annealing treatment enhances the mechanical properties of semi-crystalline polymers, particularly those with low crystallinity, such as carbon fiber PLA. Crystallinity is a significant component impacting the strength of a semicrystalline material; this is due to intrinsic polymer properties and its thermal history, such as cooling kinetics in thermal processing [66]. The ideal temperature for annealing process must be above the glass transition temperature and below the melting point to obtain changes. The deformation of specimens can be analyzed after annealing or heat-treatment experiments. Technological heating devices which are utilized by majority of scientist for the heating treatment of composites are electrical oven, microwave, temperature/environmental chamber, and hot plates [58, 62, 67].

This thesis work will describe a variety of temperature loadings subjected to CFRP composites additively manufactured using modified FDM printer to understand the difference of each temperature condition process. Additionally, the influence of temperature treatment on mechanical qualities and internal structures of printed composites by means of testing and detection technologies will be analyzed. The samples will be exposed to thermal loading with different parameters such as magnitude (sub-zero, above-zero temperature) and exposition time (continuous, cyclic).

After the manufacturing process, nine groups of CFRP specimens were thermally treated at different magnitudes (above and subzero degree Celcius) and exposition times (cyclic and prolonged). The aim of the study was to determine the relationship (influence) of the temperature on the morphological structure and mechanical behavior of the CFRP composite. On each group of thermal treatment, a mark label was given as presented in Table 3.3. The heat treatment was performed at Kaunas University of Technology, Lithuania, with a universal

environmental oven, "Memmert" Model UFB-400. A constant oxygen renewal supplied by the oven amounted to a percentage of ambient air. For the group of prolonged temperature, the specimens were placed in a preheated oven at a desired temperature and duration (i.e., 65°C for 6 hours) before being naturally cooled to room temperature.

For the thermal cyclic group, the temperature cycle regulation in the oven was manually adjusted using the controller settings based on real-time temperature readings from the thermocouples for a specific temperature range and several thermal cycles (i.e., from 50 to 70°C for six cycles) following the thermal cyclic plan. Each cycle had two desired temperatures with 10 minutes of dwelling time, a cooling rate of 2.5°C/min, and a heating rate of 1°C/min. The heating rate was controlled manually and monitored using the feedback from thermocouples to ensure the rate was consistent with the desired profile. The cooling process was set to allow the system to cool down naturally by turning off the heat source and monitoring the rate. It was assumed that the specimens would have undergone crystallization changes of polymers and cross-linking processes until their structure could be greatly altered.

Table 3.3: Sample groups

Group name	**Value**
Intact	untreated samples
HS-A	hot stable at 65°C for 6 hours
HS-B	hot stable at 145°C for 6 hours
HC-A	hot cyclic between 50°C to 70°C with 6 cycles
HC-B	hot cyclic between 140°C to 150°C with 6 cycles
CS-A	cold stable at 0°C, for 6 hours
CS-B	cold stable at -20°C, for 6 hours
CC-A	cold cyclic between 0°C to -5°C for with 12 cycles
CC-B	cold cyclic between -20°C to -15°C with 12 cycles

3.2.1 Thermal continuous at sub-zero and above-zero temperature

Continuous heating is defined as temperature exposition process onto materials at a stable temperature for a certain period of time, ideally for a few hours. Typically, specimens are placed at pre-heated chamber in which desired temperature is

hold constantly for a certain period of time. In global heating, polymeric composites are conditioned inside the environmental instruments to receive temperature exposure at all area of material. The typical annealing temperature is between above the glass transition and below the melting temperature of polymer. In case of PLA materials after printing process at the applied conditions reached only a partial attainable crystallinity degree, therefore in order to increase the degree of crystallinity post-processing annealing at elevated temperature, above Tg and below Tm, was employed [62, 66]. The ideal duration for thermal annealing is at least 30 minutes to attain a certain degree of crystallinity [68].

The experimental investigation of thermal annealing by means of microwave on specimens reported that in unidirectional CFRPs laminates with 0° ply angles, fibers aligned parallel to an electric field do not absorb microwave energy and behave as a reflective material [69]. Whereas for 90 ° ply angle, maximum microwave energy is absorbed by the perpendicularly aligned carbon fibers to electric field and it mainly comes from conduction loss in the carbon fibers. Based on some studies, microwaves do not affect the curing reaction, but rather enhance the rate of reaction by volumetric heating [67]. Gonzalez et.al proposed post-processing temperature optimization on CCFRC coupons via compaction method in order to provide the solution for the typical drawbacks of FDM printing technique [58]. Sample coupons were post-processed in the hot plates at 8 different temperatures ranging from 70°C to 270°C during 15 min (heating speed of 10°C/min). The post-processing temperature effects on microstructure, thermal stability and interlaminar properties of the printed CCFRC were analysed. When taking into consideration the dimensional precision, the microstructure, the thermal properties, and the mechanical properties of the final products, the ideal temperature for post-processing is 150°C.

AN experimental work of global heating treatment on CFRP composites as part of research internship program in Kaunas University of Technology, Lithuania was performed. There were 2 sets of samples which were subjected to the stable continuous hot temperature; 1 groups was exposed to 65°C and another group was exposed to 140°C. These temperatures were chosen in a such a way that it will be above the glass transition (Tg) temperature and below the melting temperature (Tm) of the matrix material used in the specimens. The tensile testing was performed subsequent to the heating treatment in order to examine the mechanical strength and Young's modulus of the treated specimens.

3.2.2 Thermal cyclic at sub-zero and above-zero temperature

The application of polymeric composite parts in aviation and automotive industries more likely undergo temperature fluctuations between -50°C and 130°C [70]. Structural materials exposed to this extreme environment may degrade over time, and cyclic temperature influence on mechanical behaviour of polymeric composites should be investigated. Thermal cycling can cause fatigue failure, which is a gradual kind of local damage [71]. The process of thermal cycling can lead to the onset of fatigue failure, which is a sort of gradual local damage. As a result of the fiber and matrix shrinking at different rates, thermal cycling produces thermal residual stresses. In composite laminates, residual stresses can lead to delamination, warping, and fatigue failures. Low heating and cooling rates are required to prevent the material from being subjected to thermal shock loading; nevertheless, this results in longer cycle times [72].

Parameters like temperature limits, dwell time at both temperatures and change rate between the limits are critical in thermal cycling processes [73]. Temperature limits are essential for the acceleration testing level. The larger the disparity between the boundaries, the greater the tensions they induce. However, if the limitations are excessively stringent, there is a significant chance that overstress failures will occur, resulting to premature failures that would never occur under actual use conditions. The glass transition temperature, Tg, of polymer materials is an example of a typical critical limit. A temperature limit exceeding Tg may result in an easily observable catastrophic failure, but it may also alter the failure processes to be unrealistic. In addition, it is advantageous to set the temperature limit as high as possible since, if the difference between the limits is insufficient, the test has a very low acceleration factor and the test time is quite long.

Dwelling time means how long of an exposure period is appropriate at each temperature limit. If a prolonged dwell time is employed, the duration of the test will lengthen until the number of cycles is decreased. Then again, In some instances, a long dwell period can potentially speed up the testing process if it generates structural changes that increase the stresses during temperature fluctuations. At high temperatures, polymer materials, for instance, relax or creep - the polymer chains within the material move to alleviate the stresses imposed by the high temperature. When the temperature is decreased, these alterations may result in a large increase in the stresses imposed on buildings. However, sufficient dwell time is necessary for these modifications to take place.

As thermal cycling is very expensive and time-consuming, typically only a few

(1-100) cycles may be realized [74, 75] and certain study groups achieved 200-5000 cycles [76–79]. The illustration of one cycle in heating process is shown in Figure 3.5.

Ghasemi et al. studied the effects of temperature and the number of thermal cycling cycles on residual stresses of polymeric composites at several stacking sequences during thermal cycling. One thermal cycle is a 70 °C to 100°C then back to 70°C. The heating rate is 3–5°C every minute; dwell time at both extremes of temperature is 15 min. It was reported that the condition of thermal cycling leads to a decrease in the residual stresses and an increase in the failure index. The failure index results amount can be used to determine whether or not a material will fail under loading conditions. The material fails if the failure index is equal to or greater than 1.

Guigon et al. studied mechanisms of degradation in carbon-epoxy 3D woven composites subjected to temperature cycling [80]. It was found that isothermal aging revealed thermo-impact oxidation's on matrix elasticity. In addition, thermal cycling ageing in neutral (nitrogen) and oxidative (air and oxygen) atmospheres caused microcracks in the matrix. Zhang et al. investigated thermal cycling-induced between 55°C and 120°C in carbon/epoxy braided composites experimentally and numerically. It was reported that composites and resins had less than 1% mass and volume change after 160 cycles. However, microcracks have not been found in acoustic emission and X-ray CT tests. T700s/3502 acoustic emission (AE) events have a logarithmic time-versus-temperature curve and occur periodically at low temperatures. Most events occur below 0 °C. The six-layer samples showed microcracking on X-ray CT. All three fiber directions had split fiber bundles [81]. An impact damage in CFRP coupons evolves under cyclic compression load was investigated by Bogenfield et al [82]. The specimens were impacted and exposed to various cyclic load levels ranging from 30% to 90% with a maximum of 300,000 cycles. Through ultrasonic examination, 3D scanning, and dent measuring, a variety of impacts regarding damage propagation, dent relaxing, and influence on residual strength were revealed. The majority of the specimen's damage remains constant after cyclic loading. Before final failure, impact damage spreads perpendicular to loading direction. It was shown that the delamination grew at back-side interfaces.

In attempt to investigate the thermal cyclic effect on 3D printed CFRP composite, an experimental investigation of cyclic heating and cooling treatment as part of research internship program in Kaunas University of Technology, Lithua-

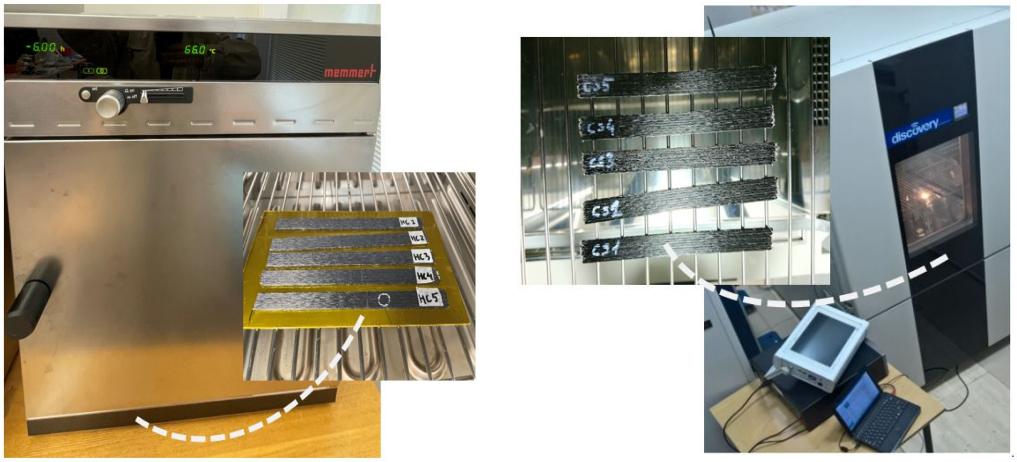

Figure 3.4: An air-circulated oven for hot temperature treatment (left) and an automated environmental chamber for cold temperature treatment (right).

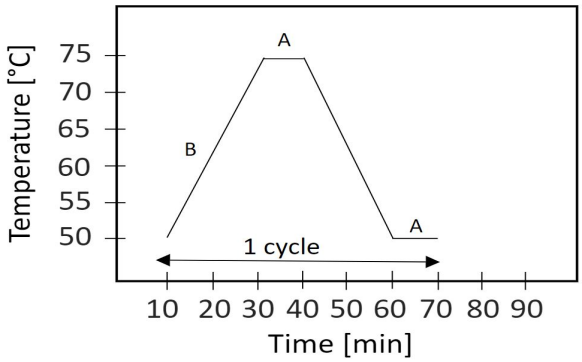

Figure 3.5: Thermal cycling profile. A=dwell time; B=heating/cooling rate

nia was performed. There were 2 sets of samples which were subjected to the cyclic hot temperature using an air-circulated environmental oven which supplied a continuous renewal of oxygen in certain percentage of ambient air. One group (HC-A) was set to have temperature range between 50 and 70 °C with the heating rate of 1°C/min and cooling rate 2.5°C/min. For another group (HC-B) which was subjected to temperature range between 140 and 150°C, the heating rate is 0.8°C/min and cooling rate of 2.2°C/min. In total there are 6 cycles for each group and dwelling time for the two extreme temperature was 10 minutes. As for the cyclic cooling treatment at negative temperature, an automated environmental chamber was utilized for 2 sets of samples in which one group (CC-A) was set to have temperature range between 0 and -5 °C and another group (CC-B) were set in a range between -15 and -20°C with 6 cycles for each group. The oven and environmental chamber devices are shown in Figure 3.4. The thermal cycling profile is shown in Figure 3.5.

3.3 Destructive testing

3.3.1 Tensile testing

After thermal treatment, tensile testing was carried out on a Tilnius Olsen H25KT universal testing machine with hydraulic grips of 25 kN. An extensometer was calibrated with a displacement rate of 2 mm/min against strain gauges to determine tensile strength and strain for all group samples. Four locations on the samples were labeled with a marker 15 mm from the center to measure the elastic strain. Gripping tabs made of PLA were printed separately, having dimensions 50 mm in length, 12.5 mm in width, and 2 mm in thickness, and each specimen was then glued with two tabs at the front side and two at the backside. Five samples were necessary to be printed for each group of thermal treatment to determine the mean value for the mechanical properties of the specimens according to the ASTM D3039 standard. The prepared PLA tabs for gripping process in tensile testing is shown in Figure 3.6 and tensile test setup are shown in Figure 3.7.

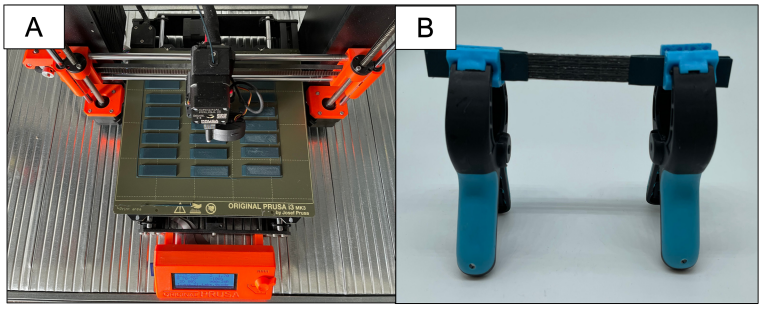

Figure 3.6: Printed PLA tabs for gripping process (A) and clamping process of the tabs to CFRP specimen (B).

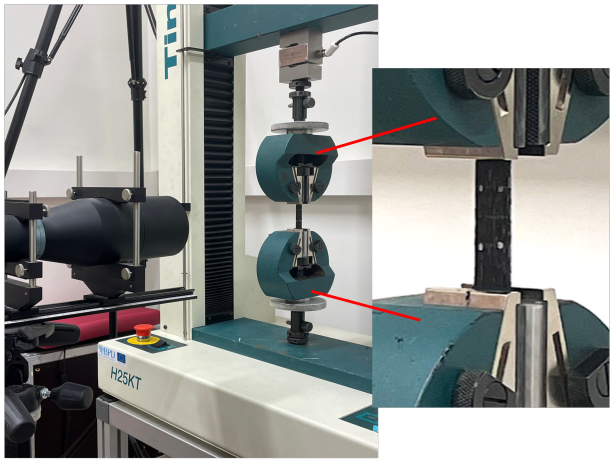

Figure 3.7: Tensile testing setup according to ASTM standard D3039.

The tensile properties of polymer matrix composite materials are determined us-

ing the ASTM D3039 standard method. This standard is used for calculating the modulus of elasticity (Young's modulus) in materials testing, particularly using the linear section of a stress-strain curve from tensile testing which represents the elastic deformation region near the failure point. The strength of each thermal group specimen was calculated using the maximum load, thickness, and width. The ultimate tensile strength (UTS) is calculated by dividing the force exerted at the failure point by the beginning of the cross-section. The tensile modulus and strength values of the CFRP specimens were calculated by Equation 3.1 and Equation 3.2, respectively.

$$\sigma = \frac{F_{max}}{A} \tag{3.1}$$

$$E = \frac{\Delta F}{A_f} . \frac{L_o}{\Delta L} \tag{3.2}$$

where F_{max} denotes the maximum tensile force given during the test (N), A_f is the cross-sectional area of the composite specimen (mm^2), ΔF and ΔL are the differences in the force and extension between two strain points, respectively, and L_0 is the gauge length of the specimen.

3.3.2 Differential Scanning Calorimetry

Differential scanning calorimetry (DSC) measures the energy absorbed (endotherm) or released (exotherm) as a function of time or temperature and it is suitable for detecting the effects of thermal degradation by observing the melting and crystallization process. The important thermal phases are studied to determine the polymer crystallinity: glass transition (Tg) following ASTM standard E1356, cold crystallization (Tcc), and melting point temperature (Tm) following ASTM standard E794. Tg is indicated by a shift of the baseline from the initial DSC curves and reported glass transition temperature was based on the observed midpoint temperature. An exothermic peak is indicating a cold crystallization where an exothermic reaction (heat release) occurred, while an endothermic peak (heat adsorption) refers to the melting temperature in which an endothermic reaction takes place.

A DSC equipment, TA Instruments Q2000, was utilized to analyze the thermal properties of CFRP specimens under controlled and isothermal conditions. The sample for each thermally treated group was chopped into small pieces and measured with a precision scale. About 10 mg of sample from each treatment group

was placed in an alumina hermetic pan and inserted into the DSC cell. A nitrogen atmosphere was supplied to the test chamber at a flow speed of 50mL/min for the cooling process, while an electrically heated furnace was used for heating. The DSC measurement for each sample consisted of two times of the heating process and one time of the cooling process. The first heating scan in DSC is used for removing the thermal history of the polymer which might have gone through during its synthesis and post processing steps. Tg value difference after the second heating run could be insignificant whereas Tm and Tc value difference could be very distinct difference in their respective values between the two runs. The DSC program is shown in Table 3.4.

Table 3.4: DSC program steps

Step	**Temperature**	**Heating rate**
Hold equilibrium	24°C	
Ramp-up	200°C	10°C/min
Hold isotherm for 2 min		
Ramp-down	40°C	10°C/min
Hold isotherm for 2 min		
Ramp-up	200°C	10°C/min

A DSC measuring cell consists of a furnace and an integrated sensor with designated positions for the sample and reference pans. The sample is placed in an aluminum pan, and the sample pan and an empty reference pan are placed on small platforms within the DSC chamber. Thermocouple sensors lie below the pans and they are connected to thermocouples. This allows for recording both the temperature difference between the sample and reference side (DSC signal) and the absolute temperature of the sample or reference side. The functional principle of an interior chamber of DSC is shown in Figure 3.8.

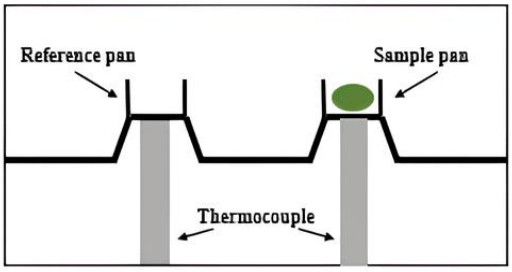

Figure 3.8: Schematic diagram of DSC interior chamber

The mechanism of the heating process between the reference pan and the sample pan is presented in Figure 3.8. When the DSC measuring cell is being heated, the reference side—typically an empty pan—heats up more quickly than the sample side because of the sample's heat capacity (C_p); for example, the reference temperature (Tr, green) rises slightly more quickly than the sample temperature (Ts, green) [83]. The two curves behave similarly while heating at a steady rate until a sample reaction occurs. In this example, the sample melts at t_1. The temperature of sample does not vary during melting; nevertheless, the temperature of the reference side remains constant and continues to rise linearly. When melting is complete, the sample temperature begins to rise again, with a linear increase commencing at time t_2.

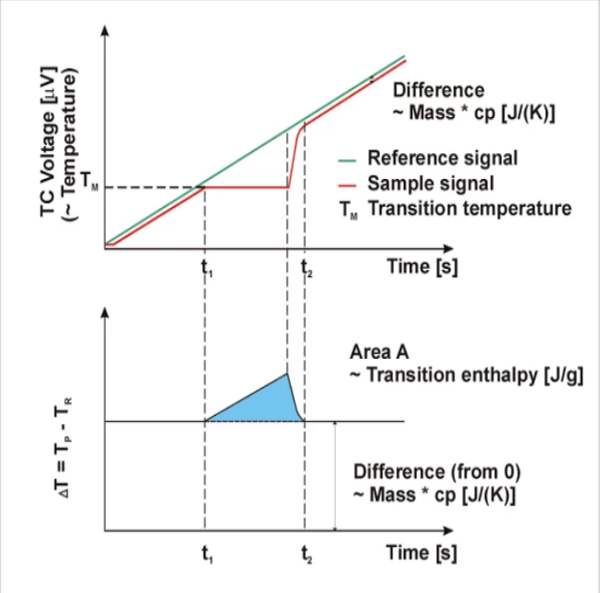

Figure 3.9: A mechanism of the heating process between the reference pan and the sample pan.

The lower part of the figure shows the differential signal (ΔT) of the two temperature curves. A blue peak, symbolizing the endothermic melting process, is produced by calculating the differences and is located in the center region of the curve. The created peak in the graphs may point upward or downward, depending on whether the reference temperature was deducted from the sample temperature or vice versa during this computation. The heat content of the transition (enthalpy in J/g) is associated with the peak area. A typical DSC thermogram is shown in schematic Figure 3.10 below.

DSC was used to determine the glass transition temperature (Tg) of the polymeric composite samples in accordance with ASTM E1356. The melting temperature and crystallization temperature will also be analyzed according to ASTM

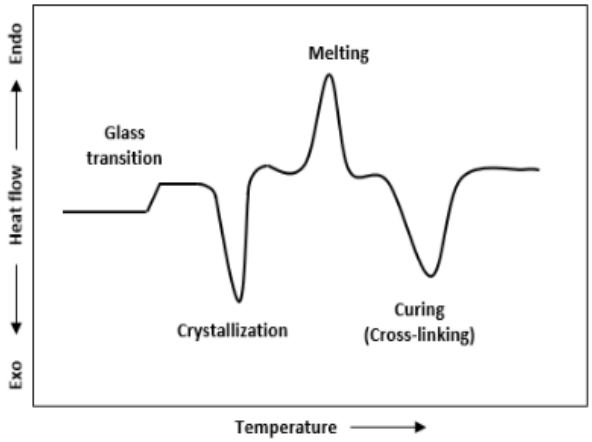

Figure 3.10: A schematic of a DSC thermogram

E794. The purpose of the test was to determine whether there was any change in crosslinking of the PLA polymer, which could signify degradation as a result of the conditioning process. A DSC equipment (TA Instruments Q2000) was used to perform thermal analysis of the composite samples under controlled and isothermal conditions. The sample for each thermally treated group was chopped into small pieces to fit inside the pan due to the stiffness of the fiber-reinforced raw filament. There were 5 groups of printed CFRP samples for various thermal treatments as summarized in Table 3.3. The prepared samples were measured with a precision scale. About 10 mg of sample from each treatment group was placed in an alumina hermetic pan and inserted into the DSC cell. A nitrogen atmosphere was supplied to the test chamber at a flow rate of 50mL/min for the cooling process while an electrically heated furnace is used for heating. The temperature was ramped from 20°C to 200°C and then cooled back to 20° C at a heating and cooling rate of 10 ° C/min. The measurement for each sample consisted of two times of the heating process and one time of the cooling process. The following program was used: hold equilibrium at 24 ° C, ramp at 10 °C/min to 200 ° C, hold isotherm for 2 min, ramp at 10 °C/min to 40 °C, hold isotherm for 2 min, and ramp back at 10 °C/min to 200 ° C. The DSC equipment and DSC cell can be seen in Fig.3.11.

Semicrystalline polymers are made up of two distinct phases: amorphous and crystalline. As a polymer becomes more crystalline, the fraction of the amorphous component decreases, and thus the change in the sample's Cp at Tg decreases. If the polymer becomes highly crystalline, the DSC instrument may eventually lose its sensitivity to detect Tg. In general, as the crystalline content of the polymer increases, so will the Tg temperature. The glass transition temperature

Figure 3.11: DSC equipment and DSC cell

is commonly abbreviated as Tg. Tg is the main characteristic transformation temperature of the amorphous phase and is produced by all amorphous (non-crystalline or semi-crystalline) materials during heating. When a hard, solid, amorphous material or component changes to a soft, rubbery, liquid phase, the glass transition phenomenon occurs. Tg is a valuable material characterization parameter that can provide very useful information about a product's end-use performance. The 'classic' Tg is observed as a stepwise endothermic change in the DSC heat flow or heat capacity.

3.4 Non-destructive testing

3.4.1 Scanning Electron Microscope

Scanning electron microscopy (SEM) analysis was carried out to evaluate the microstructure of specimens due to thermal treatment. The degradation of the constituent materials (fibers, matrix, and interface) was qualitatively evaluated using these observations. A scanning electron microscope (FE-SEM SU5000, Hitachi Co., Tokyo, Japan) was utilized to observe the micro-damage that resulted from tensile testing on various specimen groups. The largest specimen that the SEM could measure had dimensions of 80 mm $\times$ 200 mm.

3.4.2 Optical Microscope

Optical microscopy analysis was carried out to evaluate the macrostructure of specimens due to thermal treatment. Prior to the application of the cyclic and prolonged thermal loadings, the optical microscope, Nikon Eclipse LV100ND,

was used to examine the structures outfitted with a high-definition color camera (Nikon DS-Ri2). The data was prepared and processed using imaging software (NIS Elements 4.5.1.00, Nikon Europe B.V., Amstelveen, The Netherlands). The largest sample size seen under the optical microscope was 150 mm square.

3.5 Results and discussions

3.5.1 Mechanical testing

Figure 3.12 and Figure 3.13 depict the typical stress-strain curves obtained from the tensile tests of CFRP composites of the above-zero and sub-zero degrees group, respectively. The stress-strain curve for each treatment group was selected based on the tensile result of a sample which can be best used to represent the average tensile strength results. While some graphs depict a trend of linear elasticity, others began to break at elongation. This type of behavior is common in semi-crystalline polymers. When the yield strength is exceeded, the chains in the amorphous sections straighten out and stop interconnecting with one another [84].

The tensile stress-strain graphs show that the untreated composite specimen reached the highest stress level, followed by the prolonged temperature group exposed to 65°C. The lowest stress level was attained from a specimen group subjected to a cyclic temperature between 50-70°C with a considerable strain level indicating more elasticity. The premature failure of printed samples at a strain of 0.75%, despite the higher elongation at break for each constituent of fiber and PLA ($> 1\%$), is likely due to a combination of processing defects like voids and porosity, stress concentrations from geometric irregularities, residual stresses from the thermal history of printing, and the inherent anisotropy of the printed composite structure. These factors collectively contribute to a lower effective strain capacity of the printed samples compared to the individual materials.

Mechanical strength and Young's modulus

Figure 3.14 depicts the results on tensile properties of the untreated group, prolonged and cyclic thermal group for 3D-printed specimens. The trends of each printed group specimen and the range of their impacts on the tensile characteristics were displayed using bar plots with mean values. The experimental values of mechanical properties for each thermal group are shown in Table 3.5. The

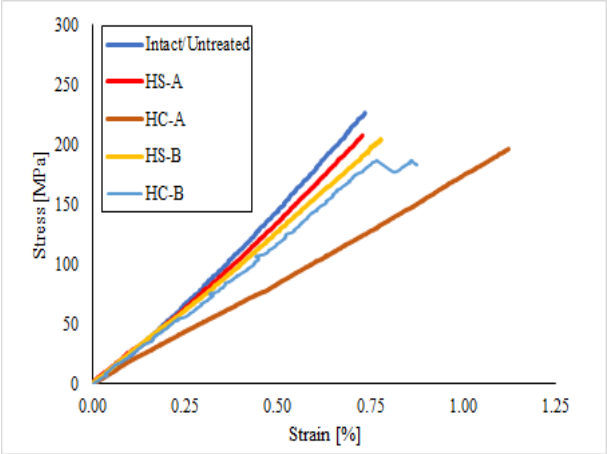

Figure 3.12: Average stress–strain curves for the samples of the above-zero group.

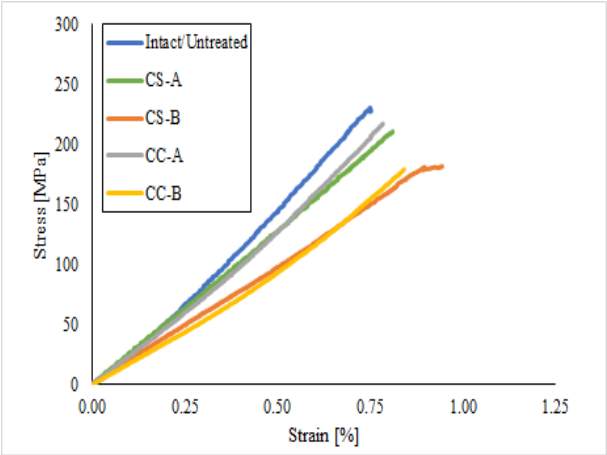

Figure 3.13: Average stress-strain curves for the samples of the sub-zero group.

untreated samples showed the highest tensile strength mean (226.14 MPa) and Young's modulus (28.65 GPa).

The tensile properties of specimens then decreased after various modes of thermal treatment at different temperature ranges. For the stable thermal treatment, the sample group treated to the above-zero temperature achieved higher ultimate tensile strength than the sub-zero temperature. The lowest Young's modulus and ultimate tensile strength were obtained from the sample group treated at -20°C. Treatment at 65°C significantly reduced the ultimate tensile strength and Young's modulus to 217.99 MPa and 25.39 GPa, respectively. However, at 145°C Young's modulus reduced to 23.97 GPa but the ultimate tensile strength of 221.21 MPa appeared to be slightly higher than the treated sample at 65°C.

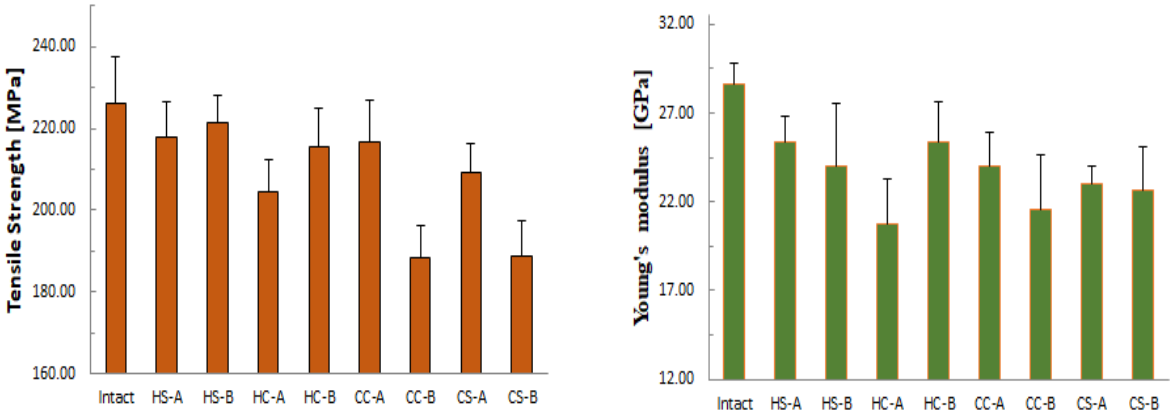

Figure 3.14: Experimental results of the tensile strength and Young's modulus of 3D-printed samples for all treatment groups.

Table 3.5: Experimental values of mechanical properties for each thermal group.

Thermal group	Tensile strength [MPa]	Young's Modulus [GPa]
Intact	226.14	28.65
HS-A	217.99	25.39
HS-B	221.21	23.97
HC-A	204.41	20.75
HC-B	215.49	25.34
CC-A	216.80	23.99
CC-B	188.32	21.60
CS-A	209.36	23.05
CS-B	188.93	22.67

The HC-B group in the thermal cycle group had strength that was essentially identical to another cyclic group with a lower temperature (HC-A), with only very tiny variances. With a Young's modulus of 25.17 GPa, the cyclic heat treatment at a higher temperature (HC-B) likewise had the highest Young's modulus, whereas the HC-A group had the lowest (20.75 GPa). The mean values in the bar plots represented the patterns of each printed group specimen and the range of their effects on tensile qualities. It is thought that the decrease in mechanical strength and elastic modulus under thermally stable and cyclic loading was caused by the difference in coefficients of thermal expansion (CTE) between the matrix and fiber. The material degraded due to the thermal stress brought on by the CTE disparity, which might lead to fibers pulling out due to fiber-matrix debonding. It is worth to mention that the large experimental standard deviations in tensile strength and modulus of CFRP composites can be attributed

to the variations of the printed specimens using the modified FDM printer despite having the same printing parameters. Inconsistent resin distribution during the impregnation process can lead to regions with different fiber-to-matrix ratios, resulting in variations of tensile properties.

The tensile tests revealed that samples exposed to prolonged high temperatures and cyclic thermal loads exhibited reduced Young's modulus and tensile strength. This mechanical degradation is consistent with the DSC findings, where reduced thermal stability (lower Tg) and altered crystallinity were observed. The mechanical properties are directly influenced by the thermal history of the samples, demonstrating that thermal treatments can significantly affect the structural integrity of the CFRP composites.

3.5.2 Differential scanning calorimetry

The DSC curves for the initial heating, cooling, and second heating cycles of intact (untreated) and thermally treated CFRP specimens at prolonged and cyclic temperatures are shown in Figures 3.15, and the values obtained from the tests are shown in Tables 3.6. The DSC curves are shown in Figure.3.15.

In the first heating process, the Tg of untreated (intact) CFRP group falls at 65°C (midpoint) and is very much close to composites treated in a stable temperature at 0°C (CS-A). The specimens exposed to a stable subzero temperature at -20°C (CS-B) have slightly higher Tg compared to intact samples. When the specimens were thermally treated repeatedly between 0°C to 5°C (CC-A), the Tg is about even higher than the CS-B group. However, with thermal cycling at extremely low temperatures between -20 to -15 °C (CC-B) the Tg value dropped to 63°C. In the case of continuous thermal treatment at high temperatures for 6 hours, specimens subjected to cyclic heating (HC-A and HC-B) possess higher Tg values compared to the stable continuous groups. This means that these groups will take a longer time required to change their material state from solid to a soft-rubbery material after the thermal treatment which makes them more brittle.

The cold crystallization (Tcc) point of the intact group is observed to be the highest among treated groups, indicated by an exothermal effect at a peak temperature of 117°C. Cold crystallization is the process of rapidly cooling a crystalline plastic from its liquid state, resulting in the freezing of polymer chains in their amorphous state. Crystallization is characterized by crystal nucleation and nucleus growth [85]. The lower magnitude of hot thermal treatment groups (HC-A and HS-A) have lower Tcc than intact specimens with values of 114°C and 98°C,

respectively.

However, cold crystallization did not occur for the higher magnitude of hot thermal treatment where the specimens were exposed to cyclic temperature (HC-B) and stable temperature (HS-B). This happens because the crystals do not have enough time to form. The formation of crystals creates an endothermic peak between the glass transition and the melting point when reheating a material in this state. The cold crystallization process is distinguished by two characteristics the promotion of nucleation as the supercooled glassy state gradually gains mobility with increasing temperature and the presence of a maximum temperature for nucleation above which the cold crystallization process is diffusion limited [86].

Table 3.6: DSC results of CFRP composite samples.

Group name	**Glass transition temperature Tg [°C]**	**Cold crystallization temperature Tcc [°C]**	**Melting temperature Tm [°C]**
Intact	64.88	117.67	158.09
HS-A	61.58	98.29	162.91
HS-B	63.23	-	161.39
HC-A	65.43	114.38	157.82
HC-B	64.19	-	164.83
CS-A	64.73	115.07	157.89
CS-B	64.61	94.88	158.92
CC-A	64.33	95.68	159.06
CC-B	62.55	94.72	158.64

It was observed that all sample groups had a double melting temperature peak during the first heating run. This is owing to the superpositioning of melting and recrystallization processes, which causes this phenomenon. When most crystallization occurs during the cool-down process, the remaining amorphous regions lack place and chain mobility, resulting in defective crystals. These defective crystals begin to melt, but almost simultaneously, recrystallization occurs, generating a new crystal structure that melts almost quickly, creating the second peak [84].

During phase transitions, CFRP samples exhibited two distinct peaks (and onset points), which may indicate more than one form or crystal structure. PLA is a polymer type used in the manufacturing process of CFRP composites, and this thermoplastic has slow crystallization kinetics. In the case of PLA, three different crystallization processes can be identified with adequate experimental

conditions: the classical cold crystallization and two processes associated with the non-reversing exotherms [87]. The DSC graphs obtained in this experiment exhibit unexpected and extraneous results, such as non-reversing heat-flow curves with two exothermic processes and a larger endotherm in the middle. The multi-exothermic processes result from several crystalline states of PLA (α and β).

The DSC curve produced lower values in the second heating process than in the first run. This phenomenon is because the relaxation or molecular rearrangement already occurred in the first heating run. The cooling process imparts/equilibrates the previously known history at a known rate from the first heating before heating again. As a result, any changes detected in the reheating curve between identical materials are not due to previous thermal history effects but rather the differences in the actual internal materials (e.g., molecular weight).

In the cooling cycle, the melt crystallization peak for each sample group can be observed and determined by the peak, which denotes the crystalline nature of the polymer. However, there are some cases when the reinforcement materials constrain the PLA chains so much that the heat capacity jump becomes undetectable in DSC. Nucleation on the sample borders, regional confinement, temperature gradient, and melt flow are all important aspects of polymer crystallization. Similarly, foreign chemicals in the pure PLA matrix affect PLA crystallization by facilitating or impeding chain movement. Furthermore, due to the presence of ordered crystallites and thicker lamellae, higher crystallinity generates higher stiffness in both materials, preventing the material from slipping into the crystal blocks [88]. In contrast, reduced crystallinity produces a higher ductility with reduced strength and stiffness [89].

DSC analysis indicated variations in Tg among samples subjected to different thermal treatments. Higher Tg values are associated with increased polymer chain mobility, suggesting better thermal stability. This stability is crucial as it correlates with improved mechanical properties, where materials with higher Tg demonstrate greater resistance to deformation under thermal stress. The degree of crystallinity, as evidenced by endothermic peaks in DSC, plays a significant role in determining the mechanical properties. Increased crystallinity generally enhances tensile strength and stiffness while potentially reducing toughness. The DSC results indicated changes in crystallinity due to thermal treatments, which are reflected in the mechanical performance of the samples.

It is worth to mention that CFRP sample maintained its shape during the 6-hour treatment at 145°C, despite this temperature being close to the melting point of

PLA, primarily due to the reinforcing role of carbon fibers. These fibers provide significant structural integrity and mechanical strength, preventing the PLA matrix from deforming significantly. Additionally, the PLA within the composite likely contains crystalline regions, which have higher melting temperatures and thus contribute to maintaining shape at elevated temperatures. The carbon fibers also aid in evenly distributing heat throughout the composite, reducing the risk of localized overheating and deformation. Furthermore, while PLA becomes soft near its melting point, its viscosity remains sufficiently high to prevent complete liquefaction, especially when reinforced by the rigid carbon fibers. Together, these factors ensure that the composite retains its structural integrity and shape during the heat treatment process.

3.5.3 Morphological analysis

Before and after the thermal loading exposures, morphological studies were carried out using an optical microscope device, and the microstructure of the various specimen groups after tensile testing was investigated using a scanning electron microscope.

Optical microscopy

Figure 3.16 presents the surface structure at the microscopic scale from each heating group that was compared before and after thermal loading to indicate the difference in the structural surface. This optical analysis was solely conducted at elevated temperatures due to its direct correlation with the thermal treatment procedure proposed post-manufacture. It is shown that the morphological surface in this experiment changed slightly before and after the thermal performance. The polymer PLA as a matrix material looked slightly finer and smoother on the prolonged and cyclic treatment samples at lower temperatures (HS-A and HS-B). However, these specimens showed no distorted shapes (some crease structure along specimen length) because of insufficient high-temperature exposure. The thermal treatment at higher temperatures showed a more obvious difference on the surface after the treatment. The case of the CFRP sample exposed to continuous heating at 145°C illustrates a dried-out of the polymer matrix, and it was confirmed by the DSC curve by a smaller area of melting peak.

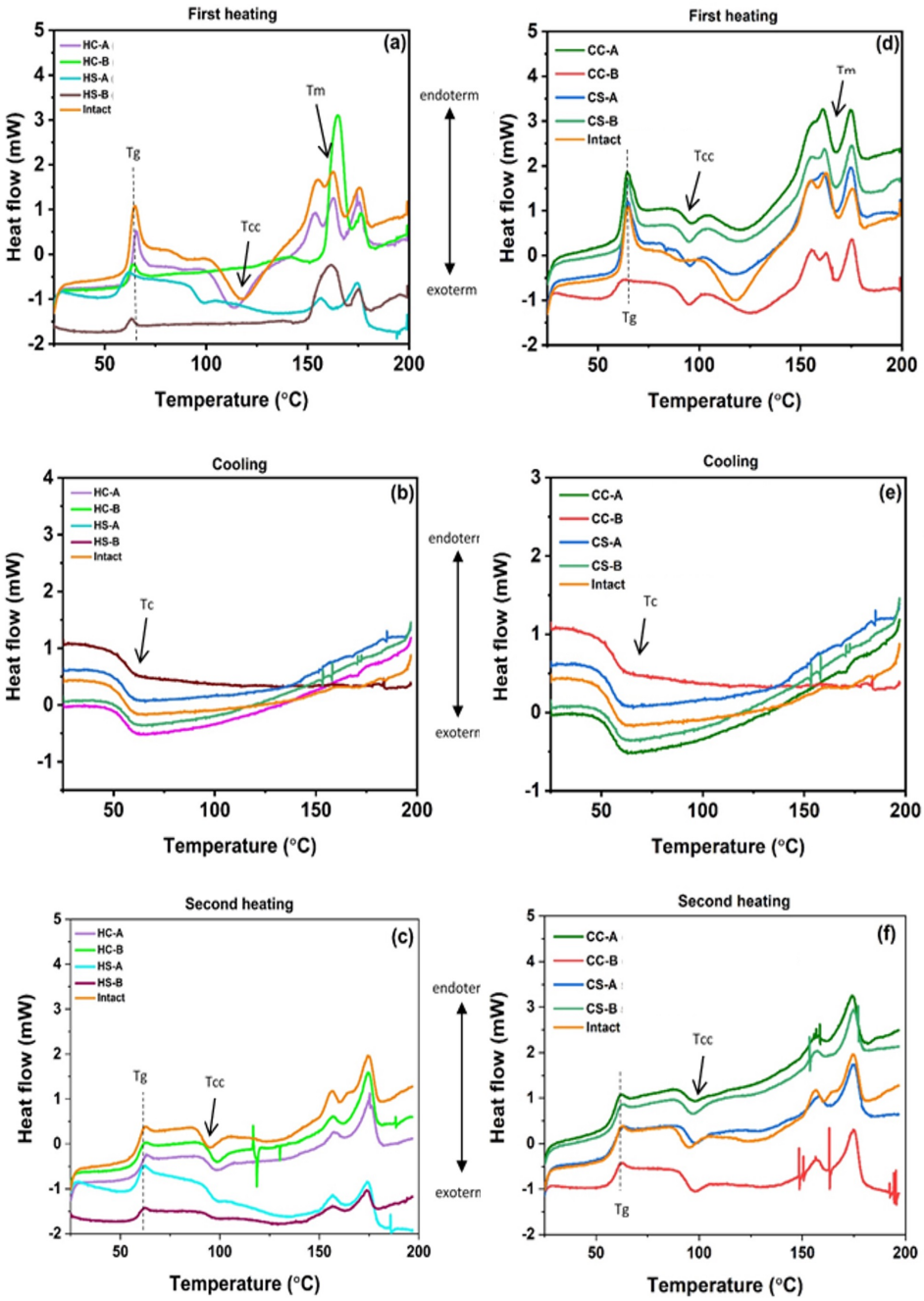

Figure 3.15: DSC graphs of 3D printed specimens for above-zero and sub-zero degrees treatment groups: first heating (a) and (d); cooling (b) and (e); and second heating (c) and (f).

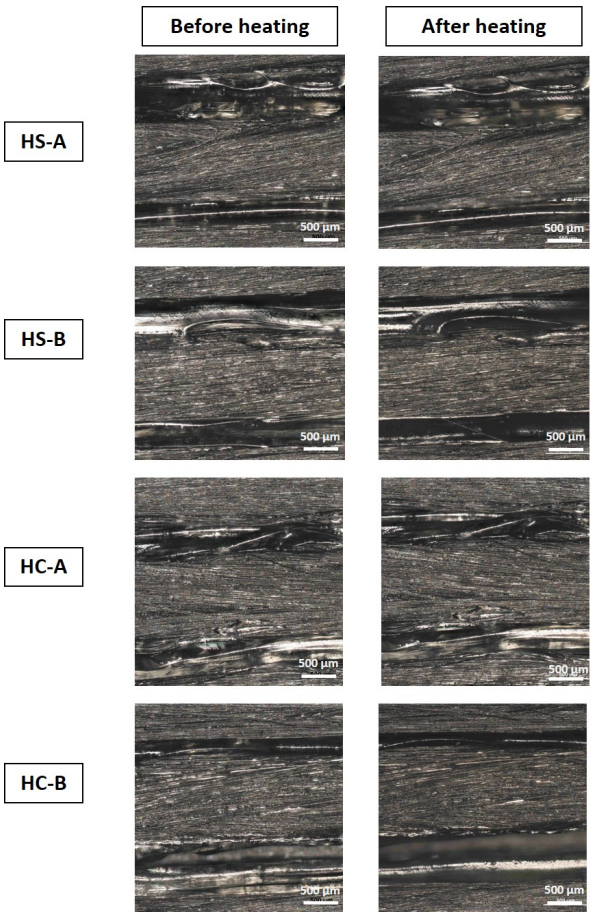

Figure 3.16: Optical micrographs of the specimen before and after the prolonged temperature at 65°C (HS-A) and 145°C(HS-B); and cyclic temperature between 50°C and 70°C (HC-A) and between 140°C and 150°C (HC-B).

Scanning electron microscopy (SEM)

The effect of thermal treatment with cyclic and prolonged temperature on the 3D-printed CFRP specimens caused morphological changes in microstructural damage after tensile testing in polymer matrix and fiber reinforcement compared to the untreated samples, as shown by the SEM micrographs in Figure 3.17. The polymer structure of the untreated sample structure displays an intact and undamaged structure, showing no signs of breakage or deterioration. Upon close examination, it exhibits a pristine surface with no observable defects or flaws. PLA polymers subjected to cyclic heating between 50°C and 70°C (HC-A) underwent significant structural degradation, evidenced by a conspicuous fracture bisecting the material. This fracture, observed prominently along the middle, suggests that the polymer experienced considerable stress and strain during the cyclic heating process, resulting in macroscopic damage. Conversely, samples subjected to cyclic thermal treatment between 140°C and 150°C (HC-B) displayed larger and more evenly distributed fractures in the polymer matrix. After prolonged thermal exposure to 145°C (HS-B), the sample exhibited matrix thinning and larger, more widespread cracks. In contrast, the polymer parts treated with prolonged temperature at 65°C (HS-A) displayed microcracks, indicating localized weakening within the material. The occurrence of microcracks implies that the PLA polymer underwent thermal expansion or contraction, leading to stress concentrations and subsequent crack formation. These findings underscore the sensitivity of PLA to temperature fluctuations and the importance of controlled processing conditions in ensuring material integrity.

It can be seen from Figure 3.17, the higher temperatures during cyclic and prolonged thermal treatments (HC-B and HS-B), exacerbate the damage to polymer components. This indicates that elevated temperatures intensify the degradation process, leading to more severe structural damage in the polymer material. The fracture appeared to exist uniformly in almost all areas of the matrix material. In addition to that the fibers were also showing some warping behavior and were no longer coated by the material made from the pre-impregnation process. This can be interpreted as the brittleness observed in the material treated at higher temperatures can be primarily attributed to the increase in crystallinity, which is a significant factor in enhancing brittleness. Crystallinity restricts the polymer chains' movement, making the material less flexible and more prone to brittle failure. This behavior is confirmed by DSC results where the cold crystallization were not presented in groups HC-A and HC-B. This is because there is no crystal

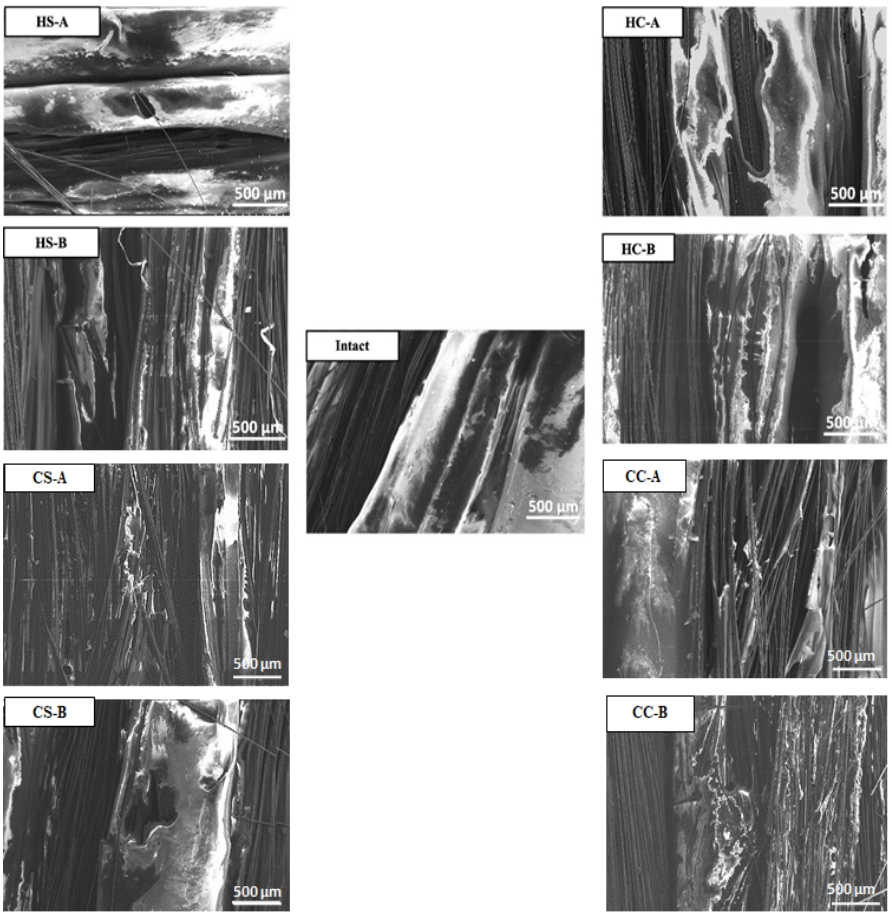

Figure 3.17: SEM photos of the untreated and treated specimen group following destructive tensile testing.

nucleation which will increase the chain mobility with the increasing temperature.

In the cold thermal treatment case, the prolonged temperature at -20°C (CS-B) created some noticeable gaps in the fibers, and matrix crack was also presented with some fiber pull-out. For the treatment at 0°C (CS-A), fibers seemed to remain in their initial arrangement and the gaps between fibers were not observed. However, the PLA matrix is slightly distorted compared to the untreated (intact) group. Fibers warping and separation were the damage resulting from thermal cycling between 0 to 5°C (CC-A). In addition to that, the matrix was observed to be deformed into some unstructured arrangement. A similar morphological structure was observed for the thermal cycling between -20 to -15°C (CC-B) where the polymer matrix was not only deformed but seemed to be more nucleated and formed some thin-small membranes.

Morphological analysis through techniques such as scanning electron microscopy (SEM) showed changes in the microstructure of the CFRP composites after thermal treatments. For instance, samples subjected to high-temperature treatments

exhibited signs of fiber-matrix debonding and matrix degradation, which are consistent with the observed reductions in mechanical strength and modulus. The morphological features provide a visual confirmation of the damage mechanisms inferred from the DSC and tensile test results. The fracture surfaces of the tensile-tested samples revealed different failure modes depending on the thermal treatment. Samples treated at higher temperatures showed brittle fracture characteristics with less fiber pull-out, indicating reduced ductility and toughness. This morphological evidence supports the findings from both the DSC and tensile analyses, illustrating how thermal history impacts the fracture behavior of CFRP materials.

Table 3.7: Observable degradation types for each thermal group.

Thermal group	Degradation types
Intact (without thermal treatment)	pristine, no polymer damage/fracture
HS-A (prolonged at 65°C)	localized micro-crack of matrix
HS-B (prolonged at 145°C)	matrix thinning and more distributed crack of matrix
HC-A (cyclic 50°C to 70°C)	macro-fracture at the middle area of matrix
HC-B (cyclic 140°C to 150°C)	widespread area of matrix fracture
CC-A (cyclic 0°C to -5°C)	fibers warping and separation
CC-B (cyclic -20°C to -15°C)	fibers warping and nucleated matrix
CS-A (prolonged at 0°C)	no fiber pull-out and gaps, matrix brittleness
CS-B (prolonged at -20°C)	fibers pull-out and gaps, matrix crack

3.6 Conclusions

This research has experimentally characterized the mechanical characteristics of 3D-printed continuous carbon fiber reinforced polymer (CFRP) composites. The unidirectional (UD) composite layers were printed using a modified FDM printer, and subsequently, the thermal treatments at various magnitudes and modes were subjected to the printed samples. To determine the mechanical characteristics, impact of temperature, and morphological structure of the specimens, thermal analysis, tensile testing, and microscopic inspection have been performed after the thermal treatment. The tensile results show that the UD CFRP samples without heat treatment demonstrate the highest mechanical behavior (strength and modulus) compared to the thermal cyclic and prolonged temperature-treated groups. The yield and ultimate tensile strength decreased for continuous and cyclic tem-

peratures when the testing temperature was raised to higher temperatures. After testing the specimens under several different thermal exposures at different magnitudes and modes, following thermal cycling, it was discovered that the treated group had less mechanical performance than the group that had been kept at a constant temperature. However, there is no direct correlation observed between higher cyclic temperature exposure and increased mechanical degradation in the materials. This suggests that factors beyond temperature alone influence the extent of mechanical damage, highlighting the complexity of material response to thermal treatments.

Based on the thermal analysis using DSC testing, glass transition temperature (Tg), cold crystallization temperature (Cc), and melting temperature (Tm) were studied. The specimens subjected to cyclic heating at hot temperatures (HC-A and HC-B) possess higher Tg values than the stable continuous groups (HS-A and HS-B). This indicates that when the subjected temperature is higher, a longer time is necessary to transform their material state from solid to soft rubbery after heat treatment, making them more brittle. The cold crystallization did not occur for a higher magnitude of hot thermal treatment where the specimens were exposed to cyclic temperature (HC-B) and stable temperature (HS-B). This happens because the crystals do not have enough time to form. The first heating produced higher thermal values than the second heating run because the cooling process imparts/equilibrates the previously known history at a known rate from the first heating before heating again. As a result, any variations in the second heating graph between identical materials are brought on by actual internal variations in the materials (such as molecular weight) as opposed to influences from the thermal history of the material. During phase transitions, CFRP samples exhibited two distinct peaks (and onset points), which may indicate more than one form or crystal structure. The double peak of melting temperatures was obtained due to the super-positioning of melting and recrystallization processes.

The morphological surface depicted in Figure 3.16 had modest changes both before and after the thermal treatment, as revealed by a visual inspection for the lower temperature of positive degrees Celcius. The thermal treatment at higher temperatures showed a more obvious difference on the surface after the treatment. The case of the CFRP sample exposed to continuous heating at 145°C illustrates a dried polymer matrix, and it was confirmed by the DSC curve by a smaller area of melting peak. Using an SEM microscope, the fracture structure of the specimens after tensile testing and structural changes in the matrix PLA from

each thermally treated and untreated group were investigated.

The findings highlight a correlation between temperature exposure and damage in polymer parts subjected to thermal treatments. Specifically, both cyclic and stable thermal treatments at above-zero degree Celcius resulted in more severe damage as temperatures increased (HC-A and HC-B). The observed brittleness of the fibers following heating suggests that they had dried out during the procedure, exacerbating their susceptibility to breakage. This phenomenon is further supported by DSC data, indicating the absence of cold crystallization in these groups due to the lack of crystal nucleation and reduced chain mobility. Conversely, cold thermal treatment at -20°C (CS-B) induced noticeable gaps in the fibers and matrix breakage with fiber pull-out, while treatment at 0°C (CS-A) maintained fiber integrity without visible gaps. These insights underscore the critical role of temperature control in preserving material integrity and inform future optimization strategies for thermal processing protocols in polymer manufacturing.

Chapter 4

Numerical method

4.1 Introduction

The numerical study was conducted to model the behavior of polymeric composites in relation to the effect of global elevated temperature on the 3D printed CFRP samples. From a macromechanical approach, the specimen was modeled as stacked solid elements at the laminate level and treated as a homogenous equivalent material. The laminate is composed of six-ply unidirectional (UD) lamina with stacking sequence (LSS) at 0 degree, and the constitutive material behavior of the laminate was treated as if it were a single orthotropic material. As symmetry planes parallel and perpendicular to the fibers, the array of carbon fibers in polymer matrix is assumed to be square. Macro-mechanical modeling was utilized to characterize the deformation and mechanical behavior of a material.

A finite element method (FEM) model was utilized to produce numerical results for a carbon fiber-reinforced polymer composite system. The geometry of the composite model was constructed as a deformable homogenous solid using the computer-aided design software ABAQUS. The model geometry has a dimensional area of 92 x 95 mm and a thickness of 2 mm. The specimen model was discretized into an eight-node trilinear heat transfer brick hexahedral mesh with C3D8T element type. There were 4416 finite elements, 19266 nodes, and 249750 degrees of freedom in the FEM model. The simulated load scenario was divided into two stages: initial step and loading step, with temperatures ranging from 10°C to 55°C with a 5°C step. The relative humidity inside the chamber was expected to be steady at 20%. During the increased heating, the numerical modeling of the CFRP composite employing the coupled temperature-displacement approach will be explored within thermo-mechanical strain analysis.

Comparing the experimental and numerical values presented in Figure **??**, the per-

centage difference between them is calculated as ca. 18%, while the average strain difference is equal to 5.7x10^{-6} m/m. The disparity between the experimental and numerical curves is due to the variability of the AM sample structure, which can be clearly seen in Figure **??** (b). The difference between those values are due to some defects which the specimen possess. Some presented voids and structure irregularity in the sample contributed to the inconsistency during the experimental measurement [3, 90]. Furthermore, the incorporation of reinforcements during FDM printing may increase the strength of the material system, but this benefit is outweighed by a poor reinforcement/matrix interaction, non-uniform reinforcement distribution, and inappropriate impregnation. These variables will result in the formation of new voids [3].

The expeditious development in the manufacturing techniques and design of new materials and structures in the engineering sector has sparked a great interest in the industry and scientific research. Additive manufacturing (AM) or three-dimensional (3D) printing is a set of manufacturing techniques that allow producing 3D components in a layer-by-layer manner. Among various AM techniques, the fused deposition method (FDM) is chosen due to its ability to print complex geometries with low cost and flexibility to use different materials. AM techniques can be used to create carbon fiber reinforced polymer (CFRP) elements which can outperform printed samples made of pure polymers. Employing carbon fibers (CFs) as reinforcement agents in polymer-based composites will make their weight remains light with increased strength.

Up to recent days, numerous experimental works have been performed to study the mechanical strength and failure effect of 3D printed CFRP specimens with various printing process parameters and printing design of expected samples such as infill pattern, infill percentage, layup orientations, etc [31, 91, 92]. In the sense of real-life application of these printed materials, such elements can be exposed to different environmental factors and temperature influence is one of the most typical. Temperature strongly influences matrix material joining together CFRP components resulting in material strength reduction. The thermal effects on the mechanical behavior of AM-printed CFRP samples have also been studied experimentally by researchers [61, 84, 93–95].

However, there are limited works to investigate the temperature effect followed by mechanical testing on additively manufactured CFRP samples by means of numerical modeling. Utilizing numerical simulation to study the thermal influence and mechanical properties will be able to extend more understanding of materi-

als characterization based on underlying theoretical/mathematical perspectives. Furthermore, the consideration of several design factors such as cost, mass, dimensional stability, and stiffness can be a constraint in the experimental outcome and it can be minimized in order to optimize the expected outcome.

The goal of the present study is to perform numerical simulations on the thermal effects and mechanical properties of unidirectional (UD) CFRP composite manufactured with the FDM method. The numerical analyses were performed using classical laminate theory (CLT) as a predictive model and finite element method (FEM) on the samples with the same alignments of the fiber reinforcement and the thickness of the fiber bundles used during the AM process. ABAQUS software is the main tool for numerical analyses presented in the thesis. The material's strength and modulus are compared for the intact (without thermal influence) sample and treated samples exposed to prolonged temperatures at 65°C and 145°C. The obtained numerical results from both approaches (CLT and FEM) are then compared with the experimental results.

In this study, there are nine models made with shell elements in FEM software, and the python scripts were generated to model the CLT. The composite was modeled asymmetric laminate with 4 plies/layers where the fibers are unidirectionally aligned in the loading direction. The first model was subjected only to tensile loading as the intact sample without thermal loading. The next models were samples subjected to the continuous (prolonged) temperature at 0°C, -20°C, 65°C, and 145°C; then an in-plane tensile mechanical loading was applied. The other models were samples subjected to the cyclic temperature between 50°C to 70°C, 140°C to 150°C, 0°C to -5°C, and -20°C to -15°C; then an in-plane tensile mechanical loading was applied. The idea of this numerical work is to determine numerically the additive-manufactured composites response (strain, stress) to the applied thermal and mechanical loads. The numerical analyses can be used instead of destructive mechanical tests for numerical models that were positively validated using experimental results.

4.2 Materials

4.2.1 Mechanical properties

The ability to accurately predict how a composite will behave under various mechanical loadings is an important aspect of the composite application. Consti-

tutive material behavior of each layer of printed part is orthotropic and similar to lamina behavior. The Rule of Mixture (ROM), is a common predictive method for two-part composites. Based on the iso-stress model, this theory proposes that the composite modulus (Ec) is a combination of the individual moduli of the fiber and matrix constituents (Ef, Em, respectively) versus their individual composite volume fractions (Vf, Vm, respectively) [96]. The following assumptions are made by the ROM theory: uniform fiber dispersion, perfect bonding between fiber and matrix, and void-free matrix [96]. The selected mechanical properties of composites are listed in Table 4.1. E11 and E22 denote elastic modulus along and transverse to fiber direction, respectively; G12 is shear modulus, $\nu 12$ is Poisson's ratio, and ρ is the density of CFRP composites.

Table 4.1: Mechanical properties of composite

$E_{11}[MPa]$	$E_{22}[MPa]$	$G_{12}[MPa]$	ν_{12}	ρ[t/mm^3]
43.753x10^3	2.823x10^3	2.844x10^3	0.2818	13.35x10^{-4}

4.2.2 Thermal properties

For a transversely isotropic material such as a UD-reinforced fibrous composite, the determination of thermal conductivity in the composite material can be predicted by rule of-mixtures type expression [97]. The parallel thermal conductivity in the axial direction (longitudinal to fiber) can be predicted by a ROM type expression by Behren [97]. For transverse thermal conductivity, the calculation takes into account the fact that the interface region may have a different thermal conductance than the matrix or the fiber referring to the formula by Hasselman and Johnson [98]. The parallel thermal conductivity in the axial direction (longitudinal to fiber) and the series conductivity in the transverse direction (perpendicular to fiber) are calculated using formula in Equation 4.1 and Equation 4.2, respectively:

$$\kappa_{11} = V_f \kappa_f + V_m \kappa_m \tag{4.1}$$

$$\kappa_{22} = \frac{\kappa_f \kappa_m}{V_m \kappa_m + V_f \kappa_f} \tag{4.2}$$

While for heat capacity of composite is calculated using the following Equation 4.3:

$$C_v = \frac{(V_f \rho_f C_f + V_m \rho_m C_m)}{\rho} \tag{4.3}$$

The indexes f and m means fibre and matrix, respectively. V is the volume and ρ means density.

The following are the basic assumptions considered in the thermal case based on Schapery formulation [99]:

- fibre and matrix are assumed to be isotropic and linear elastic.
- The strains in the longitudinal direction are the same in the matrix and in the fibres (Voigt assumption)
- The stresses in the transverse direction are constant (Reuss assumption)
- The homogenised macroscopic stresses in the lamina are zero, i.e. the assumption δL = δ T = 0 is used.

Thermal properties of the CFRP composite are collected in Table 4.2.

Table 4.2: Thermal properties of the CFRP composite

$\alpha_{11}[m/mK]$	$\alpha_{22}[m/mK]$	$\kappa_{11}[W/mK]$	$\kappa_{22}[W/mK]$	$C_v[J/kgK]$
$2.37x10^{-6}$	$7.15x10^{-5}$	1.93	0.16	1370

4.3 Finite element modeling (FEM)

Thermal influence plays a critical role in CFRP composites' mechanical performance because they can cause significant variations in material properties and structural responses. At the microscale, the interaction between carbon fibers and the polymer matrix is greatly influenced by temperature changes, affecting interfacial bonding, stiffness, and strength. On the macroscale, temperature fluctuations can lead to dimensional changes, stress concentrations, and even structural failures. Temperature has a strong influence on the matrix material used to join CFRP components, resulting in a reduction in material strength. This happens because the polymer becomes gradually softer when subjected to temperature above the glass transition temperature (Tg) of the polymer matrix material. Changing the temperature of the composite also causes swelling or contraction of the polymer matrix, which the fibers resist. This causes residual stresses to form and changes the distribution of stress and strain in the composite [100]. Due to the different expansion or contraction behavior of the constituent laminates, a similar effect is observed at the laminate level.

4.3.1 Micromechanical modeling

The microstructure has become increasingly more complex for reinforced materials due to the variety of fiber architecture and layer stacking configurations. Micromechanical analysis allows for a detailed insight to the mechanical behavior of a composite by considering the influence of each constituent [**meiro2016**]. The approach used in this thesis is based on a representative volume element (RVE) or unit cell concept which acts as a representative of the entire microstructure. The boundary value problem on the structural scale and in the microstructural scale (RVE) is solved by the Finite Element (FE) method. Within this approach, the chosen RVE method is using non-homogenization where the RVE is not being solved each time before performing the macrostructural model but rather a separate modeling step. The elastic properties of each constituent is computed for solving the microstructural mechanical performance. Compared to the homogenization methods where the elastic properties of the microstructure are obtained solving the microstructural problem, their computational cost for a non-linear analysis is high because it is required solving the RVE in every integration point at the macrostructural problem.

Generally, a considerable amount of voids exist in the composite printed parts during the manufacturing process. In order to properly model the printed composite, FEM modeling based on homogenized methods and real microstructure can be used. In the homogenized models, the effective properties of printed parts are considered and the rasters are not explicitly molded [3]. In the real microstructure method, the analysis domain is considered.

Homogenization techniques are used to evaluate the constitutive behavior of composites from the properties and geometric features of its constituents. In these methods, a representative volume element (RVE) representing the periodic structure of the material is considered for the numerical analysis along with periodic boundary conditions [3]. The RVE is a cubic unit cell with single or multiple particles (inclusion, ellipses or fiber) embedded randomly or uniformly in the polymer matrix with a certain volume fraction similar to those of the printed composite. To generate this RVE, different algorithms were implemented in order to define a distribution of the particles in the space [12]. Somireddy et al. used these techniques to evaluate the constitutive behavior of the printed parts by applying periodic boundary conditions [101, 102]. The response of two RVE domains under the axial strain was illustrated and the calculated constitutive behavior is well-agreed with experimentally observed behavior.

Unit cell generation

The unit cell generation is created based on regular square packing for the unidirectional (UD) composites with ordered fiber distribution with transverse isotropy behavior which most such UD composites possess owing to the fiber distribution in the matrix over the cross-section perpendicular to fibers. The square packing has been chosen to minimize the size of the unit cell using the reflectional symmetries, however, loads in terms of macroscopic stresses or strains can only be applied individually and an arbitrary combination of the macroscopic stress components is usually not allowed. In this simulation, the simplest case with circular fiber and perfect bonding will be considered. A general scenario has been sketched in Figure 4.1 in which regular fiber cross-section is illustrated schematically.

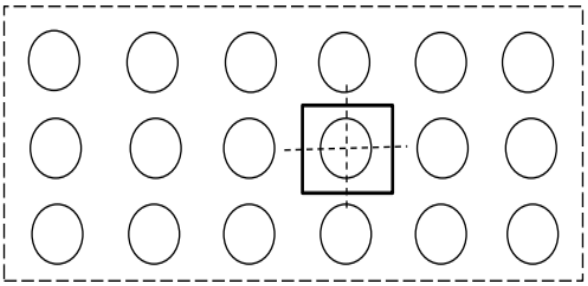

Figure 4.1: A regular packing of square unit cell.

To correctly predict the mechanical behavior of a composite ply, the individual models for the constituents must be calculated proportional to the volume fraction of the fiber to generate the RVE. The microstructure of the UD composite ply in this research was simplified as a regular, square array fiber arrangement and is a common RVE geometry to represent UD composites [103]. To explicitly define and model the interface, a layer of elements was created around each fiber. Figure 1 shows the detail of the RVE used in this research. The area of the unit cell is A = length (L) x width (W). When fibers are of a circular cross-section, assuming the diameter of the fibers to be D_f, the fiber volume fraction (V_f) for this packing can be given as in Equation 4.4.

$$V_f = \frac{N\pi {D_f}^2}{4LW} \tag{4.4}$$

The volume fraction (V_f) of the carbon fiber reinforcement content was 18.2%. To provide an idea of the compactness of the packing in this case, the maximum theoretically achievable fiber volume fraction is f = $\pi/4 \approx 78.54\% when the radius of the fibers = half of the spacing between fibers$.

Mesh and Boundary conditions

The meshes for a unit cell employed to analyze the RVE are shown in Figure 4.3 with a 18.2% fiber volume fraction. The meshes generated with the size of 14.3 are all converged. Quadratic quadrilateral elements are used for the matrix part while for the fiber part quadratic triangular elements are used for generating the mesh.

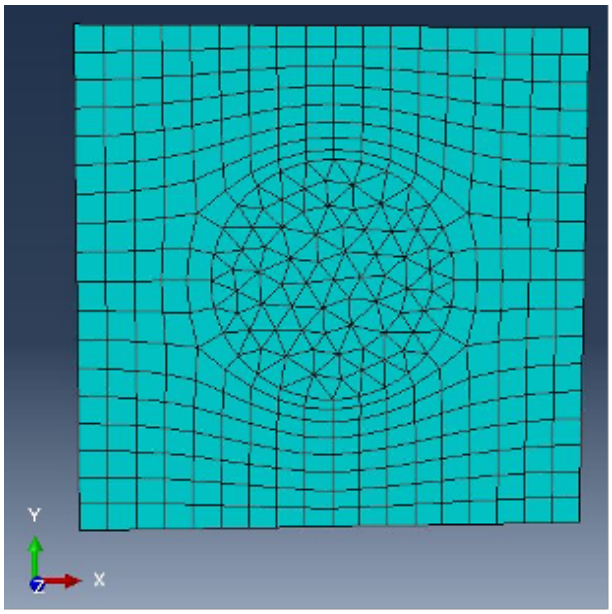

Figure 4.2: Generated meshes for a unit cell.

Different loading conditions are applied to the generated unit cell to mimic the same loading history and study the mechanical response of composite ply in the experimental investigation. For simulating the samples subjected to heat treatments, the boundary conditions created for this simulation consist of two different loadings as thermal and mechanical. While for the intact samples, only mechanical loading is considered in the boundary condition.

For the simulation of thermal loading, amplitude tables are created with magnitude and duration for respective thermal group specimens according to the thermal loading plan similar to experimental work. The samples will have two different heat transfer schemes. The first step is thermal radiation from the temperature chamber to the sample's surface, followed by heat conduction throughout material constituents. The heat sample module in Abaqus was used in conjunction with the heat transfer physics, and the reference temperature at the boundaries was set to 0°C. The temperature is subjected within the node-set for the entire unit cell with corresponding amplitudes.

For the tensile loading simulation, the loads are applied similarly to the actual tensile test requiring appropriate boundary conditions which should be prescribed along all the

sides of the unit cell. The translational symmetry transformations from one side of the unit cell namely S1 is used to obtain boundary conditions along these sides. This one side is chosen respectively in the z-axis or U3 direction where the axial tensile loading is applied to the unit cell. The reference point (RP1) is created in order to obtain the stress and strain distribution by translating the loading from tensile pulling movement within S1. Rigid body motions with displacements in three coordinate directions have been constrained in the following Equation 4.5. The rotations about the y and z-axes are constrained by fixing the rotation of the x-axis about these axes. This can be achieved naturally if the x-axis is chosen to be attached to the longitudinal direction of fibers. Furthermore, the rotation around the x-axis is constrained by fixing the rotation of the y-axis about the x-axis.

$$U_1 = U_2 = U_3 = \frac{\partial U_1}{\partial x} = \frac{\partial U_2}{\partial y} = \frac{\partial U_3}{\partial z} = 0 \tag{4.5}$$

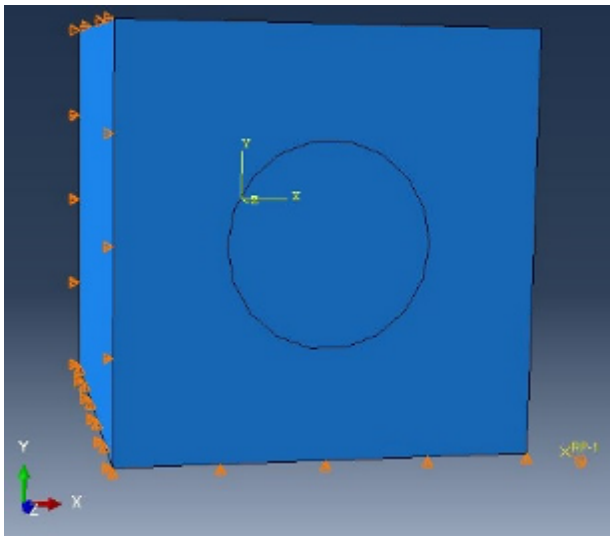

Figure 4.3: Boundary conditions for a unit cell.

4.3.2 Macromechanical modeling

The procedure to simulate thermal loading and mechanical testing using Abaqus software as finite element tools was described. The sample geometries were based on ASTM standard D3039 for tensile testing. Initially, nine finite element models were created and their material properties were defined. The unidirectional specimen geometry and its material properties calculated through ROM prediction will be incorporated into the model. There are two steps applied to the specimen model thermal and mechanical loading steps. Eight specimen models were simulated with thermal load, then followed

by mechanical load, and one model was simulated with only tensile loading (intact) as a reference for the mechanical degradation analyses. It is worth mentioning that in the step module, the thermal step must be specified before the tensile step to mimic the experimental behavior properly. Boundary conditions (BC) were used to constrain model parts to remain fixed (non-displacing) or to move by a certain amount.

Specimen model

The rectangular specimen geometry was modeled according to testing standard ASTM D3039 having dimension equivalent to which experimental work has been done, with standard analytical approaches and numerical modeling techniques (i.e. orthotropic shell) for uniaxial tensile loading case. The investigated structure is comprised of a combination of matrix and fibers. In this work, the material properties of the composite were calculated using the rule of mixture (ROM), a theoretical model by Voight. The individual volume fractions for matrix PLA and continuous carbon fiber (CCF) are obtained from the experiment. Then the specimen model was discretized into linear quadrilateral elements with four-node, reduced integration with hourglass control, and finite membrane strains within the thermally coupled thin shell, S4RT type. The FEM model consisted of 784 finite elements and 891 nodes. The geometry of the tensile test specimen is a unidirectional carbon fiber laminate with a rectangular cross-section, 150 mm in length, 13 mm in width, and 2 mm in thickness, and 45 mm on either end for grasping. The geometry of the test specimen is intended to resemble the actual geometry.

Thermal step

The simulations of thermal loading at stable continuous temperature have been performed for nine specimen models as representative of each thermal group. The samples will have two different heat transfer schemes. The first step is thermal radiation from the temperature chamber to the sample's surface, followed by heat conduction between material layers. The heat sample module in Abaqus was used in conjunction with the heat transfer physics, and the reference temperature at the boundaries was set to 0°C. The initial temperature at all nodes is 20°C, and the bottom face has a constant temperature of 20°C throughout the simulation. The sample model's boundary conditions are determined by how it interacts with its external surroundings in order to accurately represent the physical phenomena of the experimental setup, which may insulate the edges. The heat was applied to the laminate's top surface and is distributed from the top layer (layer 1) to the bottom layer (layer 4) with the Stefan-Boltzmann constant = 5.67 x 10-8 $Wm^{-2}K^{-4}$ and emissivity $\epsilon = 0.96$ [104]. Furthermore, the sample orientation was aligned with the global axis, which identifies the different faces of the

laminate. The specimen model and its boundary conditions for the thermal loading are presented in Figure 4.4. It is worth mentioning that the convection heat transfer was not considered. In the environmental chamber, the temperature is controlled by an electric heater, where the mechanism of heat exchange is propagated through electromagnetic waves. Thus there exists no heat flow that can be brought to the wall of the sample or taken away from it. With the initial value problem now in a suitable format, the equations were discretized to yield the finite element equations. The final step is to adopt an isoparametric approach and introduce the appropriate quadrature scheme, which will be able to solve the equations numerically.

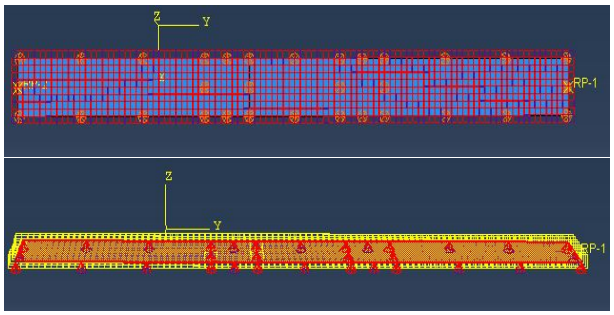

Figure 4.4: A representative model for thermal exposure (continuous at 65°C at the entire sample (left) and boundary condition at the bottom (right).

Mechanical step

Stress analyses were performed on the developed finite element model of the composite specimen under static load. The boundary conditions and loads are applied similarly to the actual tensile test, so that the experimental work is replicated. The boundary conditions for tensile test simulation are set to be fixed or clamped (encastred) in all directions in the lower grip, and free in the direction of the applied load in the upper grip (unconstrained in the longitudinal direction). These options ensure that the tensile test simulation is as accurate as possible, with no rotations or bending. The upper grip load was applied using surface traction, and the magnitude was calculated using the appropriate maximum force possessed by each specimen group, which was then distributed uniformly with the general traction type. When a simple structure, such as a composite plate, breaks due to applied forces, it fails fast because the load increases as the structure's load carrying capacity falls. When a mechanical force applied to a thin composite plate causes it to break, the structure fails relatively quickly because the load increases as the structure's load-carrying capacity decrease. When using displacement-controlled loading, the weight of the structure decreases as it fails, allowing for a slower rate of failure. The tensile test specimen model with boundary and loading conditions is presented in Figure 4.5.

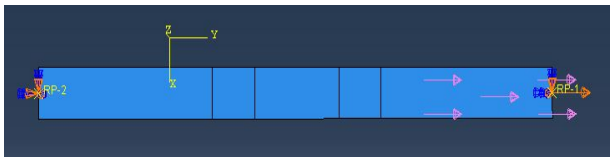

Figure 4.5: Model specimen for the tensile test with boundary and loading conditions

4.3.3 Results and discussion

The mechanical response of printed CFRP samples after thermal treatment and without thermal treatment has been simulated with FEM software at the microscale and macroscale. Figure 4.6 shows the stress distribution of a unit cell after tensile testing, after thermal exposure, and after thermal-tensile loading. It can be observed that in Figure 4.6a, when only tensile loading is applied the stress is very much concentrated in the fiber cell than matrix due to the stiffness behavior of the fiber. When thermal loading applied to the unit cell gives the different magnitudes of stress distribution in the matrix and fiber cell as shown in Figure 4.6b, this is due to the elasto-plasticity behavior and higher thermal expansion of the polymer and carbon fiber. In the Figure 4.6c, with the thermal and tensile loading the stress distribution in the matrix and fiber are more varied due to the anisotropy behavior of the CFRP unit cell.

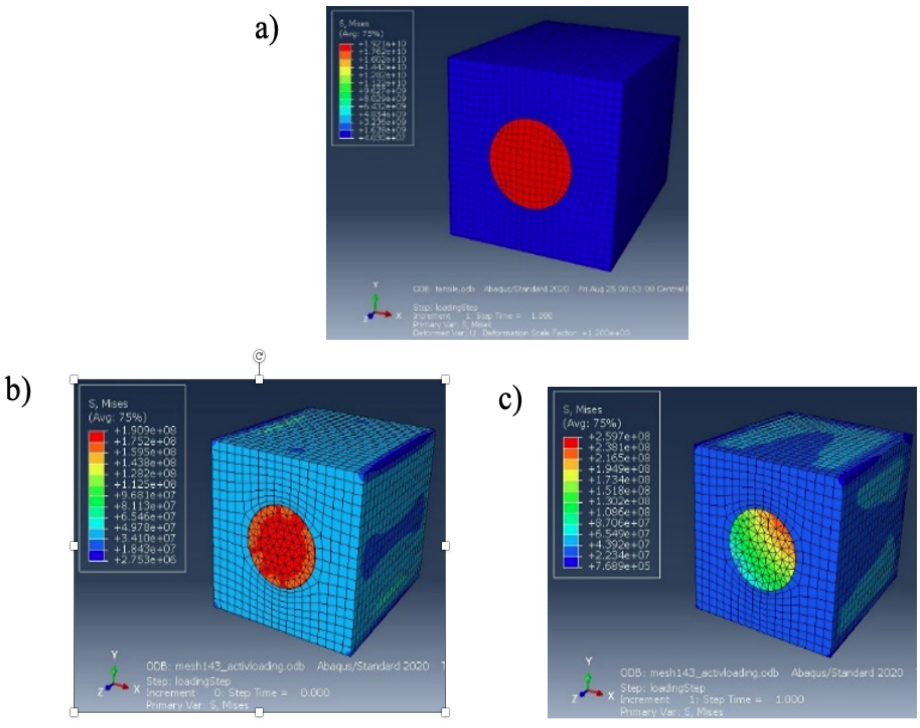

Figure 4.6: (a) after tensile loading without thermal treatment; (b) after thermal loading; (c) after tensile loading with thermal treatment.

The numerical results at the macroscale level for the specimen under the tensile test are presented in Figure 4.7, 4.8, and 4.9. The maximum displacement occurred at the free end and the reaction force was found to be maximum at the clamped end for both models. Analyses of laminated shells subjected to a thermal gradient through the thickness with material properties dependent on temperature and different boundary conditions are reported here as additional results are not currently available in the literature. Mechanical stress and strain under thermal loads for CFRP composites consisting of 4 plies of material are examined using the FEM model and compared with experimental results.

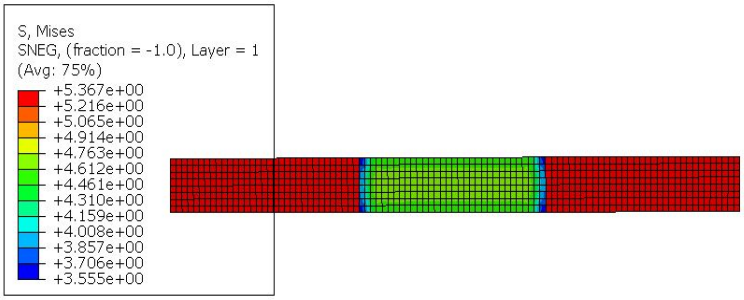

Figure 4.7: Stress of CFRP model HS-A during tensile testing

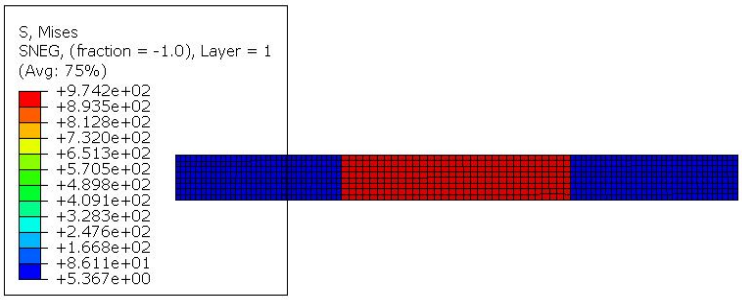

Figure 4.8: Stress of CFRP model HS-A after tensile testing

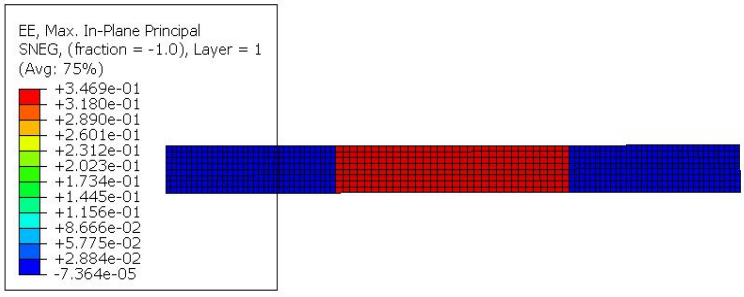

Figure 4.9: Strain of CFRP model HS-A after tensile testing

The tensile strength and Young's modulus of each sample group were compared between experimental values with the values obtained from microscale and macroscale simulation as shown in Table 4.3 and Table 4.4, respectively.

Table 4.3: Young's modulus with FEM modeling

	Young's Modulus [GPa]		
Group	Experimental	Microscale	Macroscale
Intact	28.65 ± 1.14	30.24	28.72
HS-A	25.39 ± 1.45	27.965	26.73
HS-B	23.97 ± 3.54	26.23	22.07
HC-A	20.75 ± 2.55	22.12	21.87
HC-B	25.34 ± 2.31	27.60	27.13
CC-A	23.99 ± 1.97	25.12	22.76
CC-B	21.60 ± 3.05	23.40	23.44
CS-A	23.05 ± 1.01	25.87	24.21
CS-B	22.67 ± 2.39	25.02	24.34

Table 4.4: Tensile strength with FEM modeling

	Tensile strength [MPa]		
Group	Experimental	Microscale	Macroscale
Intact	226.14 ± 11.43	235.82	232.21
HS-A	217.99 ± 8.44	224.37	222.34
HS-B	221.21 ± 6.69	227.23	225.13
HC-A	204.41 ± 8.07	206.32	209.02
HC-B	215.49 ± 9.61	218.21	218.89
CC-A	216.80 ± 10.05	220.40	220.20
CC-B	188.32 ± 8.05	190.77	200.52
CS-A	209.36 ± 6.97	213.21	215.12
CS-B	188.93 ± 8.54	191.22	202.24

It can be seen that the strength and modulus values from the microscale gives less accurate prediction than macroscale simulation compared to the experimental values after the thermal loading. Simulation at micromodel can be improved with homogenization technique and the macroscale model can be improved by modeling a bridge simulation at mesoscale to obtain more desired results. The mechanical properties from both microscale and macroscale overestimate the experimental result. It is assumed that the defects in CFRP samples resulted from the nature of the FDM printing method affecting the lower mechanical properties values in the experiment. The efficiency analysis from both scales reveals that microscale FEA simulation gives computational saving

because of the easier modeling stage and smaller model size in the preprocessing where it can reduce solving time during the processing.

It is confirmed that the samples subjected to a higher temperature (145°C) possess lower mechanical strength and modulus than the lower one (65°C). Meanwhile, an intact sample not exposed to any temperature loading performs the highest mechanical properties. The slightly overestimated modeling is obtained due to the simulation approach at the macro-scale model; where the residual stress of composite materials at the micro-mechanics level has not been considered.

4.4 Classical Laminate Theory

Classical laminate theory (CLT) was used to calculate the thermal stress from the curing process after the manufacturing stage is completed. The formulation of CLT was written in a python script and the necessary elastic and modulus properties were computed into the script for the calculation.

4.4.1 Theory

CLT is supported by two fundamental assumptions (First-Order Shear Deformation Theory). First, the deformation of the laminate in the thickness direction is negligible ($\epsilon_z = 0$). A straight line in the undeformed configuration remains straight after the deformation of the laminate. In addition, interlaminar shear strains are assumed to be negligible ($\gamma_{xz} = \gamma_{yz} = 0$) and will not be taken into account in the derivations of CLT. This implies that a straight line normal to the midplane remains perpendicular to the midplane after deformation (Kirchoff theory). This assumption is valid for thin laminates in which the shear moduli of the plies is not very low (e.g. foam cores of sandwich panels).

From this hypothesis, the kinematic relation between laminate deformations (mid-plane strains and curvatures) and ply deformations is derived:

$\{\epsilon(\mathrm{z})_{xy}\} = \{\ \epsilon^0\ \} + \mathrm{z}\ .\{\kappa\}$

The reduced stiffness matrix Qij for each material used in the laminate defines the elastic behavior of the ply in-plane loading. When a laminate uses only one type of composite material, there will be only 1 stiffness matrix. The in-plane load vector (N) is balanced by integrating the stresses along the thickness of the laminate. Combining the kinematic relation and ply mechanics, the following expression is obtained:

$\{\mathrm{N}\} = [\mathrm{A}]\ \{\ \epsilon^0\} + [\mathrm{B}]\ \{\kappa\}$

The out-of-plane load vector (M) is balanced by integrating the moments along the thickness of the laminate. As in the previous explanation, combining the kinematic relation and ply mechanics, the following expression is obtained:

$\{M\} = [B]\ \{\epsilon^0\} + [D]\ \{\kappa\}$

Finally, in-plane and out-of-plane loads and deformation are found to be coupled according to the following system of equations:

$$\begin{Bmatrix} N \\ M \end{Bmatrix} = \begin{bmatrix} A & B \\ B & D \end{bmatrix} \begin{Bmatrix} \epsilon^0 \\ \kappa \end{Bmatrix}$$

where submatrices A, B and D are defined by the laminate stacking sequence and elastic properties of the plies. Matrix A denotes the extensional stiffness, B denotes the coupling stiffness and D is the bending stiffness of the laminate. In the case of symmetric laminates, the B matrix is null, so in-plane and out-of-plane loads and deformations are uncoupled yielding 2 independent systems of equations:

$$\Big\{N\Big\} = \Big[A\Big]\ \Big\{\{\epsilon^0\}\Big\}$$
$$\Big\{M\Big\} = \Big[D\Big]\ \Big\{\{\kappa\}\Big\}$$

4.4.2 Results and discussion

Generally, CLT theory gives an idea about the force distribution in the laminate and the deformations those forces may cause in the CFRP composite. Understanding and verifying the behavior of composite laminates such as deformation mechanisms and stresses would be easier with CLT analyses. Having the equations to solve the kinematic relation between strain and stress on CFRP laminate and the generated python script to calculate the stiffness matrix (Q), then the elastic strain and stress values at each ply could be obtained. Applying kinematic conditions to the system yields a relationship between strain and displacement in the laminate equations. Furthermore, generalized Hooke's Law is used to obtain a relationship between the stresses generated as a result of the strains developed. A stiffness matrix is generated, which serves as a constant in defining the stresses and strains mentioned above.

By adding these stresses and moments in different directions, the resultant is obtained. Finally, to relate these resultant stresses to the external force applied, equilibrium conditions are used that govern the underlying equations. In order to get the relationship between the external forces and the corresponding displacements of the laminate, the equations are re-substituted. In the case of unidirectional printed samples, the symmetric laminates formula under uniaxial in-plane load was used. Therefore, the out-of-plane deformation is not observed which makes the B matrix zero values and the curvature

(κ) is also 0 while the global strain is the same for all the plies. The required thermal and material properties to be computed are α_1, α_2, E_1, E_2, G_{12}, G_{23}, V_{12}.

After computing the thermal and material properties, the number of layers, the layers orientation, and thickness size; the A, B, and D matrices are then calculated. The stress and strain values obtained from CLT computation at global and local coordinates are the same since the laminate consists of unidirectional plies (0/0)s. Thermal stress induced after the thermal loading was calculated by subtracting the final temperature of the sample from the curing temperature (where the room temperature occurred). The stress and strain values obtained from CLT computation at global and local coordinates are the same since the laminate consists of unidirectional plies (0/0)s [105]. A comparison between numerical and experimental results (Young's Modulus) is presented in Table 4.5. The shown results indicated that CLT overestimates strength values when compared to experimental results because, in CLT theory, it is assumed that a modeled composite structure should have no defects while in fact, the final printed specimens possess some imperfection.

Table 4.5: Young's modulus and tensile strength modeled with CLT analyses

	Young's Modulus [GPa]		Tensile strength [MPa]	
Group	Experimental	CLT analyses	Experimental	CLT analyses
Intact	28.65 ± 1.14	28.24	226.14 ± 11.43	234.31
HS-A	25.39 ± 1.45	27.18	217.99 ± 8.44	223.24
HS-B	23.97 ± 3.54	26.08	221.21 ± 6.69	226.14
HC-A	20.75 ± 2.55	23.10	204.41 ± 8.07	206.22
HC-B	25.34 ± 2.31	27.33	215.49 ± 9.61	219.42
CC-A	23.99 ± 1.97	24.67	216.80 ± 10.05	221.42
CC-B	21.60 ± 3.05	22.79	188.32 ± 8.05	193.11
CS-A	23.05 ± 1.01	24.23	209.36 ± 6.97	214.12
CS-B	22.67 ± 2.39	24.55	188.93 ± 8.54	192.33

4.5 Conclusions

The widely known methods for thin composite laminate have been studied using CLT theory for the analytical approach. This theory does not behave in relation to laminate thickness because of its relatively small thickness. The results showed that CLT overestimates strength values when compared to experimental results because CLT theory assumes that a modeled composite structure should have no defects, whereas the final

printed specimens do have some porosity. CLT is recommended for research because it only applies to thin plates with a length-over-thickness ratio greater than 40.

The numerical approach compares FEM modeling calculations with experimental results obtained by using Abaqus software based on the layered shell element. The slightly overestimated modeling results from the simulation approach at the macro-scale model, which does not account for the residual stress of composite materials at the micro-mechanics level. The 3D shell element type and size were chosen based on mesh refinement precision and high computation efficiency when compared to other element types. This basically means that with those element types, a very coarse mesh (e.g., 5 mm in the x-direction) can be chosen without sacrificing much precision while significantly increasing computation efficiency. Attempts to compute higher-order element types were made during simulation, and the results showed a higher variance in results for different mesh sizes, as well as a highly inefficient computation time when compared to the average.

FEM and CLT are both effective methods for analyzing thermomechanical behavior. The difference between numerical and experimental work could be due to imperfections such as porosity, imperfect bonding between plies, or micro-cracks in carbon fibers in a laminated composite that can cause delamination. However, given the scarcity of literature on additively manufactured CFRP composites at various temperatures, such as sub-zero, this simulation work will be expanded into a multiscale approach in the near future, and the specimens model will be subjected to a range of temperatures. However, there is a bigger discrepancy between the obtained FEM results compared to values obtained from the CLT model. This could be due to the mesh size selected which requires high computational time for the simulation to be completed. Therefore, some elements might not be considered in the result database file.

Chapter 5

Conclusions and Future work

5.1 Conclusions

The aim of the PhD thesis was achieved because it successfully investigated the effects of various thermal treatments on the mechanical properties, thermal stability, and morphological characteristics of continuous carbon fiber reinforced polymer (CFRP) composites fabricated using a modified FDM printer. Through comprehensive experimental and analytical approaches, the study revealed how different thermal conditions, such as prolonged heating and cyclic thermal exposure, significantly degrade the mechanical performance of CFRP composites. This degradation was evident in reduced tensile strength and modulus, as well as changes in thermal properties like glass transition temperature (Tg) and crystallinity, which were meticulously analyzed using Differential Scanning Calorimetry (DSC) and other methods.

The thesis of the dissertation has been proven because the research provided concrete evidence that thermal treatments affect the structural integrity and performance of CFRP composites. The combination of optical and scanning electron microscopy (SEM) revealed substantial morphological changes, including matrix thinning, cracks, and fiber pull-out, especially in samples subjected to high-temperature treatments. These observations were supported by DSC analysis, which indicated altered thermal transitions correlating with reduced mechanical properties. Furthermore, numerical simulations using FEM modeling with ABAQUS software complemented the experimental results, demonstrating consistency between theoretical predictions and practical findings. This alignment of experimental data with numerical models validates the hypothesis that optimized thermal management is crucial for maintaining the mechanical and thermal integrity of CFRP composites.

The novelty of the thesis lies in its integrated approach to studying CFRP composites using both experimental and numerical methods. This research is pioneering in its

use of a modified FDM printer to fabricate CFRP composites and its comprehensive analysis of how thermal treatments influence these materials. The innovative combination of non-destructive testing (NDT) and destructive methods to characterize thermal, morphological, and mechanical properties provides a deeper understanding of the degradation processes in additively manufactured CFRP composites. Moreover, the study's findings offer valuable insights and practical guidelines for the design and manufacturing of high-performance composite materials, highlighting the critical importance of thermal management during processing and application.

Referring to the thorough literature review as well as the results of numerical and experimental analysis, several innovative elements can be identified in the thesis. These are as follows:

- Development of a numerical model of CFRP structure under a variety of thermal treatments. This model enabled the prediction and analysis of thermal effects on mechanical properties, facilitating the understanding of degradation mechanisms and performance outcomes in CFRP composites.
- Construction of measurement stands at IMP PAN and KTU for analyses of thermal loading influences on AM CFRP structures. These stands were equipped with advanced sensors and data acquisition systems to accurately capture thermal responses and mechanical performance changes.
- Modification of the test stand for tensile tests at KTU to be used for AM CFRP samples. The existing test stand for tensile testing at KTU was modified to accommodate and accurately test additively manufactured CFRP samples. These modifications included the implementation of fixtures and grips designed specifically for the unique characteristics of AM CFRP, ensuring reliable and precise tensile strength measurements.
- Comprehensive analyses of thermal degradation processes in AM CFRP samples were conducted using both non-destructive testing (NDT) techniques and destructive methods. These analyses provided detailed insights into the effects of thermal treatments on the structural integrity, revealing critical information on changes in mechanical properties, morphological alterations, and the onset of damage mechanisms.
- The study successfully identified and determined the dominant types of degradation processes that occur in AM CFRP samples following specific thermal loadings. By correlating the observed mechanical and morphological changes with different thermal conditions, the research pinpointed key

degradation mechanisms, such as increased brittleness and matrix cracking, that significantly impact the performance of the material.

The study underscores the critical importance of integrating theoretical results with practical experiments, emphasizing their intrinsic interrelationship. The influences of various thermal treatments on the mechanical properties, thermal stability, and morphological characteristics of continuous carbon fiber reinforced polymer (CFRP) composites printed using the modified FDM printer were analyzed. It is possible to characterize the thermal, morphological, and mechanical properties of CFRP composites printed by modified FDM printer using NDT and destructive methods. This integration is particularly essential in the context of composite material structures, where practical experiments are indispensable due to the unique anisotropic properties of the materials and susceptibility to damage mechanisms such as cracks and delamination. It is possible to determine the degradation processes of AM CFRP using the combination of experimental and numerical approach. The findings of this investigation serve as a valuable guide for selected techniques, including an analytical program for the thermomechanical analysis of composite plates, and provide a detailed and comprehensive reference on several key aspects.

5.2 Future works

Building upon the findings of this dissertation, future research will further explore the mechanical and thermal degradation of carbon fiber reinforced polymer (CFRP) composites fabricated via additive manufacturing. Specific areas of focus will include:

(a) Extended Thermal Exposure Studies: Conducting long-term thermal exposure experiments to better understand the degradation kinetics of CFRP composites at both above- and sub-zero temperatures. This will include a broader range of thermal cycles and durations to simulate more diverse environmental conditions.

(b) Advanced Characterization Techniques: Utilizing additional characterization methods such as X-ray computed tomography (XCT) and atomic force microscopy (AFM) to gain deeper insights into the microstructural changes and damage mechanisms in CFRP composites post-thermal treatment.

(c) Impact of Environmental Factors: Investigating the combined effects of thermal exposure and environmental factors such as humidity and UV radiation on the mechanical properties and thermal stability of additively manufactured CFRP composites.

(d) Material Modifications: Exploring the incorporation of different types of carbon fibers and matrix materials to enhance the thermal and mechanical performance of CFRP composites. This includes experimenting with novel additives and surface treatments to improve interfacial bonding and reduce thermal degradation.

For the numerical analysis, future work will aim to address the discrepancies observed between the finite element method (FEM) and classical laminate theory (CLT) models, particularly in the context of additively manufactured CFRP composites. The following areas will be prioritized:

(a) Multiscale Modeling Approaches: Expanding the simulation work to include a multiscale modeling approach, which will incorporate both macro- and micro-scale analyses to account for imperfections such as porosity, imperfect bonding between plies, and micro-cracks in the carbon fibers.

(b) Enhanced FEM Simulations: Improving FEM simulations by incorporating more detailed material models and temperature-dependent properties. This includes the development of advanced constitutive models that can accurately capture the anisotropic and nonlinear behavior of CFRP composites under varying thermal conditions.

(c) Comparative Analysis with CLT: Conducting a comprehensive comparative analysis between FEM and CLT models across a wider range of temperatures and mechanical loading conditions to better understand the sources of discrepancies and refine the accuracy of both methods.

(d) Validation with Experimental Data: Continuously validating numerical models with extensive experimental data to ensure reliability and accuracy. This will involve close collaboration between experimental and numerical research teams to iteratively improve model predictions.

(e) Simulation of Sub-Zero Temperatures: Extending simulations to perform more extreme sub-zero temperature conditions (at much lower magnitudes), which are currently underexplored in the literature. This will provide a more complete understanding of the thermal and mechanical behavior of additively manufactured CFRP composites across the full spectrum of operational temperatures.

By addressing these areas, future research will contribute to a more comprehensive understanding of the degradation mechanisms and performance characteristics of CFRP

composites, ultimately leading to the development of more robust and reliable materials for advanced engineering applications.

Bibliography

[1] Quan, C., Han, B., Hou, Z., et al. 3d printed continuous fiber reinforced composite auxetic honeycomb structures. *Composites Part B: Engineering* 187 (2020), p. 107858.

[2] Ngo, T. D., Kashani, A., Imbalzano, G., et al. Additive manufacturing (3D printing): A review of materials, methods, applications and challenges. *Composites Part B: Engineering* 143 (2018), pp. 172–196.

[3] Penumakala, P. K., Santo, J., and Thomas, A. A critical review on the fused deposition modeling of thermoplastic polymer composites. *Composites Part B: Engineering* (2020).

[4] Sachs, E., Cima, M., and Cornie, J. Three dimensional printing: rapid tooling and prototypes directly from a CAD model. *CIRP annals* 39.1 (1990), pp. 201–204.

[5] Mohamed, O. A., Masood, S. H., and Bhowmik, J. L. Optimization of fused deposition modeling process parameters: a review of current research and future prospects. *Advances in Manufacturing* 3(1) (2015), pp. 42–53.

[6] Kousiatza, C. and Karalekas, D. In-situ monitoring of strain and temperature distributions during fused deposition modeling process. *Materials & Design* 97 (2016), pp. 400–406.

[7] Wang, X., Jiang, M., Zhou, Z., et al. 3D printing of polymer matrix composites: A review and prospective. *Composites Part B: Engineering* 110 (2017), pp. 442–458.

[8] Wickramasinghe, S., Do, T., and Tran, P. FDM-based 3D printing of polymer and associated composite: A review on mechanical properties, defects and treatments. *Polymers,* 12(7) (2020), p. 1529.

[9] Singh, S., Ramakrishna, S., and Singh, R. Material issues in additive manufacturing: A review. *Journal of Manufacturing Processes* 25 (2017), pp. 185–200.

[10] Bellehumeur, C., Li, L., Sun, Q., and Gu, P. Modeling of bond formation between polymer filaments in the fused deposition modeling process. *Journal of manufacturing processes* 6(2) (2004), pp. 170–178.

[11] Sun, Q, Rizvi, G., Bellehumeur, C., and Gu, P. Effect of processing conditions on the bonding quality of FDM polymer filaments. *Rapid prototyping journal* (2008).

[12] El Moumen, A., Tarfaoui, M., and Lafdi, K. Additive manufacturing of polymer composites: Processing and modeling approaches. *Composites Part B: Engineering* 171 (2019), pp. 166–182.

[13] Council, N. R. Accelerated Aging of Materials and Structures: The Effects of Long-Term Elevated Temperature Exposure. *Washington DC: The National Academic Press.* (1996).

[14] Wickramasinghe, S., Do, T., and Tran, P. FDM-based 3D printing of polymer and associated composite: A review on mechanical properties, defects and treatments. *Polymers* 12(7) (2020), p. 1529.

[15] Nath, S. D. and Nilufar, S. An Overview of Additive Manufacturing of Polymers and Associated Composites. *Polymers* 12(11) (2020), p. 2719.

[16] Huang, Q. *3D printing shrinkage compensation using radial and angular layer perimeter point information.* US Patent 9,886,526. 2018.

[17] Ngo, T. Introduction to composite materials. *Composite and Nanocomposite Materials From Knowledge to Industrial Applications* (2020).

[18] Barbero, E. J. *Finite element analysis of composite materials using Abaqus.* CRC press, 2013.

[19] Campbell, F. C. *Structural composite materials.* ASM international, 2010.

[20] Ning, F., Cong, W., Qiu, J., et al. Additive manufacturing of carbon fiber reinforced thermoplastic composites using fused deposition modeling (FDM). *Composites Part B: Engineering* 80 (2015), pp. 369–378.

[21] Tekinalp, H. L., Kunc, V., Velez-Garcia, G. M., et al. Highly oriented carbon fiber–polymer composites via additive manufacturing. *Composites Science and Technology* 105 (2014), pp. 144–150.

[22] Love, L. J., Kunc, V., Rios, O., et al. The importance of carbon fiber to polymer additive manufacturing. *Journal of Materials Research* 29(17) (2014), pp. 1893–1898.

[23] Ferreira, R. T. L., Amatte, I. C., Dutra, T. A., and Burger, D. Experimental characterization and micrography of 3D printed PLA & PLA reinforced with short carbon fibers. *Composites Part B: Engineering* 124 (2017), pp. 88–100.

[24] Matsuzaki, R., Ueda, M., Namiki, M., et al. Three-dimensional printing of continuous fiber composites by in-nozzle impregnation. *Scientific reports,* 6(1) (2016), pp. 1–7.

[25] Ashby, M. F. and Johnson, K. *Materials and design: the art and science of material selection in product design.* Butterworth-Heinemann, 2013.

[26] Akhoundi, B., Behravesh, A. H., and Bagheri Saed, A. Improving mechanical properties of continuous fiber reinforced thermoplastic composites produced by FDM 3D printer. *Journal of Reinforced Plastics and Composites* 38(3) (2019), pp. 99–116.

[27] Heidari-Rarani, M., Rafiee, A., and Zahedi, A. Mechanical characterization of FDM 3D printing of continuous carbon fiber reinforced PLA composites. *Composites Part B: Engineering* 175 (2019), p. 107147.

[28] Tian, X., Liu, T., Yang, C., et al. Interface and performance of 3D printed continuous carbon fiber reinforced PLA composites. *Composites Part A: Applied Science and Manufacturing* 88 (2016), pp. 198–205.

[29] Goh, G. D., Dikshit, V., Nagalingam, A. P., et al. Characterization of mechanical properties and fracture mode of additively manufactured carbon fiber and glass fiber reinforced thermoplastics. *Materials & Design* 137 (2018), pp. 79–89.

[30] Dickson, A. N., Barry, J. N., McDonnell, K. A., and Dowling, D. P. Fabrication of continuous carbon, glass and Kevlar fibre reinforced polymer composites using additive manufacturing. *Additive Manufacturing* 16 (2017), pp. 146–152.

[31] Maqsood, N. and Rimašauskas, M. Characterization of carbon fiber reinforced PLA composites manufactured by fused deposition modeling. *Composites Part C: Open Access* 4 (2021), p. 100112.

[32] Li, N., Li, Y., and Liu, S. Rapid prototyping of continuous carbon fiber reinforced polylactic acid composites by 3D printing. *Journal of Materials Processing Technology* 238 (2016), pp. 218–225.

[33] Zhang, W., Cotton, C., Sun, J., et al. Interfacial bonding strength of short carbon fiber/ ABS composites fabricated by fused deposition modeling (FDM). *Composites Part B: Engineering* 137 (2018), pp. 51–59.

[34] Shofner, M., Lozano, K, Rodríguez-Macías, F., and Barrera, E. Nanofiber-reinforced polymers prepared by fused deposition modeling. *Journal of applied polymer science* 89(11) (2003), pp. 3081–3090.

[35] Sweeney, C. B., Lackey, B. A., Pospisil, M. J., et al. Welding of 3D-printed carbon nanotube polymer composites by locally induced microwave heating. *Science advances* 3(6) (2017), e1700262.

[36] Boparai, K., Singh, R, Fabbrocino, F, and Fraternali, F. Thermal characterization of recycled polymer for additive manufacturing applications. *Composites Part B: Engineering* 106 (2016), pp. 42–47.

[37] Dürager, C. Model-based damage feature extraction for structural-health monitoring applications (2018).

[38] Caminero, M., García-Moreno, I, Rodríguez, G., and Chacón, J. Internal damage evaluation of composite structures using phased array ultrasonic technique: Impact damage assessment in CFRP and 3D printed reinforced composites. *Composites Part B: Engineering* 165 (2019), pp. 131–142.

[39] Chen, Y., Peng, X., Kong, L., et al. Defect inspection technologies for additive manufacturing. *International Journal of Extreme Manufacturing* 3(2) (2021), p. 022002.

[40] Munoz, V., Valès, B., Perrin, M., et al. Damage detection in CFRP by coupling acoustic emission and infrared thermography. *Composites Part B: Engineering* 85 (2016), pp. 68–75.

[41] Moody, J. *The relationship between SHM, CM and NDT*. URL: `https://www.bindt.org/forums/moodys-memoranda/the-relationship-between-shm-cm-and-ndt/`. (accessed: 16.07.2021).

[42] Ostachowicz, W., Soman, R., and Malinowski, P. Optimization of sensor placement for structural health monitoring: A review. *Structural Health Monitoring* 18(3) (2019), pp. 963–988.

[43] Cai, J., Qiu, L., Yuan, S., et al. "Structural health monitoring for composite materials". In: *Composites and their applications*. IntechOpen, 2012.

[44] Grassia, L., Iannone, M., Califano, A., and D'Amore, A. Strain based method for monitoring the health state of composite structures. *Composites Part B: Engineering* 176 (2019), p. 107253.

[45] Maurizi, M., Slavič, J., Cianetti, F., et al. Dynamic measurements using FDM 3Dprinted embedded strain sensors. *Sensors,* 19(12) (2019), p. 2661.

[46] Wang, W., Li, L., Fan, Y., and Jiang, Z. Piezoelectric transducers for structural health monitoring of joint structures in cylinders: A wave-based design approach. *Sensors* 20(3) (2020), p. 601.

[47] Barski, M., Kędziora, P., Muc, A., and Romanowicz, P. Structural health monitoring (SHM) methods in machine design and operation. *Archive of Mechanical Engineering* 61.4 (2014).

[48] Abbas, M. and Shafiee, M. Structural health monitoring (SHM) and determination of surface defects in large metallic structures using ultrasonic guided waves. *Sensors* 18(11) (2018), p. 3958.

[49] Roach, D. P. *FAA Research Program Webinar Series on Structural Health Monitoring-Module 1: Introduction to SHM and Implementation.* Tech. rep. Sandia National Lab.(SNL-NM), Albuquerque, NM (United States), 2016.

[50] Long, J., Nand, A., and Ray, S. Application of spectroscopy in additive manufacturing. *Materials* 14(1) (2021), p. 203.

[51] McManus, H. Stress and damage in polymer matrix composite materials due to material degradation at high temperatures. In: *35th Structures, Structural Dynamics, and Materials Conference*. 1996, p. 1395.

[52] Ray, S. and Cooney, R. P. "Thermal degradation of polymer and polymer composites". In: *Handbook of environmental degradation of materials*. Elsevier, 2018, pp. 185–206.

[53] Addepalli, S., Zhao, Y., Roy, R., et al. Non-destructive evaluation of localised heat damage occurring in carbon composites using thermography and thermal diffusivity measurement. *Measurement,* 131 (2019), pp. 706–713.

[54] Haridas, A, Song, C, Chan, K, and Murukeshan, V. Nondestructive characterization of thermal damages and its interactions in carbon fibre composite panels. *Fatigue & Fracture of Engineering Materials & Structures* 40(10) (2017), pp. 1562–1580.

[55] Bowles, K. J., Jayne, D., and Leonhardt, T. A. Isothermal aging effects on PMR-15 resin (1992).

[56] Rimašauskas, M., Kuncius, T., and Rimašauskienė, R. Processing of carbon fiber for 3D printed continuous composite structures. *Materials and Manufacturing Processes* 34.13 (2019), pp. 1528–1536.

[57] Tian, X., Liu, T., Yang, C., et al. Interface and performance of 3D printed continuous carbon fiber reinforced PLA composites. *Composites Part A: Applied Science and Manufacturing* 88 (2016), pp. 198–205.

[58] Pascual-González, C, San Martín, P, Lizarralde, I, et al. Post-processing effects on microstructure, interlaminar and thermal properties of 3D printed continuous carbon fibre composites. *Composites Part B: Engineering* 210 (2021), p. 108652.

[59] Abderrafai, Y., Mahdavi, M. H., Sosa-Rey, F., et al. Additive manufacturing of short carbon fiber-reinforced polyamide composites by fused filament fabrication: Formulation, manufacturing and characterization. *Materials & Design* 214 (2022), p. 110358.

[60] Ivey, M., Melenka, G. W., Carey, J. P., and Ayranci, C. Characterizing short-fiber-reinforced composites produced using additive manufacturing. *Advanced Manufacturing: Polymer & Composites Science* 3.3 (2017), pp. 81–91.

[61] Nassar, A., Younis, M., Elzareef, M., and Nassar, E. Effects of Heat-Treatment on Tensile Behavior and Dimension Stability of 3D Printed Carbon Fiber Reinforced Composites. *Polymers* 13.24 (2021), p. 4305.

[62] Arjun, P, Bidhun, V., Lenin, U., et al. Effects of process parameters and annealing on the tensile strength of 3D printed carbon fiber reinforced polylactic acid. *Materials Today: Proceedings* (2022).

[63] Magri, A. E., El Mabrouk, K., Vaudreuil, S., and Touhami, M. E. Mechanical properties of CF-reinforced PLA parts manufactured by fused deposition modeling. *Journal of Thermoplastic Composite Materials* 34.5 (2021), pp. 581–595.

[64] Benwood, C., Anstey, A., Andrzejewski, J., et al. Improving the impact strength and heat resistance of 3D printed models: structure, property, and processing correlationships during fused deposition modeling (FDM) of poly (lactic acid). *Acs Omega* 3.4 (2018), pp. 4400–4411.

[65] Hart, K. R., Dunn, R. M., Sietins, J. M., et al. Increased fracture toughness of additively manufactured amorphous thermoplastics via thermal annealing. *Polymer* 144 (2018), pp. 192–204.

[66] Wach, R. A., Wolszczak, P., and Adamus-Wlodarczyk, A. Enhancement of mechanical properties of FDM-PLA parts via thermal annealing. *Macromolecular Materials and Engineering* 303.9 (2018), p. 1800169.

[67] Naik, T. P., Singh, I., and Sharma, A. K. Processing of polymer matrix composites using microwave energy: A review. *Composites Part A: Applied Science and Manufacturing* (2022), p. 106870.

[68] Srithep, Y., Nealey, P., and Turng, L.-S. Effects of annealing time and temperature on the crystallinity and heat resistance behavior of injection-molded poly (lactic acid). *Polymer Engineering & Science* 53.3 (2013), pp. 580–588.

[69] Zhou, J., Li, Y., Zhang, M., et al. Effect of lay-up configuration on the microwave absorption properties of carbon fiber reinforced polymer composite materials. *Materials Today Communications* 26 (2021), p. 101960.

[70] Lafarie-Frenot, M., Rouquie, S, Ho, N., and Bellenger, V. Comparison of damage development in C/epoxy laminates during isothermal ageing or thermal cycling. *Composites Part A: Applied Science and Manufacturing* 37.4 (2006), pp. 662–671.

[71] Ghasemi, A., Tabatabaeian, A, and Moradi, M. Residual stress and failure analyses of polymer matrix composites considering thermal cycling and temperature effects based on classical laminate plate theory. *Journal of Composite Materials* 53.21 (2019), pp. 3021–3032.

[72] Lüders, C. and Sinapius, M. Fatigue of fibre-reinforced plastics due to cryogenic thermal cycling. *Journal of Composite Materials* 53.20 (2019), pp. 2849–2861.

[73] Nyarko, F. K., Takyi, G., Amalu, E. H., and Adaramola, M. S. Generating temperature cycle profile from in-situ climatic condition for accurate prediction of thermo-mechanical degradation of c-Si photovoltaic module. *Engineering Science and Technology, an International Journal* 22.2 (2019), pp. 502–514.

[74] Dutta, P. K. and Hui, D. Low-temperature and freeze-thaw durability of thick composites. *Composites Part B: Engineering* 27.3-4 (1996), pp. 371–379.

[75] Grogan, D. M., Leen, S. B., Semprimoschnig, C., and Brádaigh, C. Ó. Damage characterisation of cryogenically cycled carbon fibre/PEEK laminates. *Composites Part A: Applied Science and Manufacturing* 66 (2014), pp. 237–250.

[76] Kim, R. Y., Crasto, A. S., and Schoeppner, G. A. Dimensional stability of composite in a space thermal environment. *Composites science and technology* 60.12-13 (2000), pp. 2601–2608.

[77] Gupta, S. K. and Hojjati, M. Thermal cycle effects on laminated composite plates containing voids. *Journal of Composite Materials* 53.4 (2019), pp. 489–501.

[78] Adams, D. S., Bowles, D. E., and Herakovich, C. T. Thermally induced transverse cracking in graphite-epoxy cross-ply laminates. *Journal of reinforced Plastics and composites* 5.3 (1986), pp. 152–169.

[79] Lafarie-Frenot, M. and Ho, N. Influence of free edge intralaminar stresses on damage process in CFRP laminates under thermal cycling conditions. *Composites Science and Technology* 66.10 (2006), pp. 1354–1365.

[80] Guigon, C, Lafarie-Frenot, M., Pannier, Y, et al. Impact of temperature and thermal cycling ageing on performance of 3D woven composites whit polymer matrix manufactured by RTM. In: *European Conference on Composite Materials (ECCM16), Seville, Spain*. Vol. 22. 2014, p. 26.

[81] Zhang, C., Binienda, W. K., Morscher, G. N., et al. Experimental and FEM study of thermal cycling induced microcracking in carbon/epoxy triaxial braided composites. *Composites Part A: Applied Science and Manufacturing* 46 (2013), pp. 34–44.

[82] Bogenfeld, R. and Gorsky, C. An Experimental Study of the Cyclic Compression after Impact Behavior of CFRP Composites. *Journal of Composites Science* 5.11 (2021), p. 296.

[83] Functional principle of a heat-flux DSC. *Netzsch.* Retrieved January 20 (2024), from analyzing–testing.netzsch.com/en/landingpages/principle–of–a–heat–flux–dsc.

[84] Handwerker, M., Wellnitz, J., Marzbani, H., and Tetzlaff, U. Annealing of chopped and continuous fibre reinforced polyamide 6 produced by fused filament fabrication. *Composites Part B: Engineering* 223 (2021), p. 109119.

[85] Turnbull, D. Formation of crystal nuclei in liquid metals. *Journal of Applied Physics* 21.10 (1950), pp. 1022–1028.

[86] Muravyev, N. V. and Vyazovkin, S. The status of pyrolysis kinetics studies by thermal analysis: Quality is not as good as it should and can readily be. *Thermo* 2.4 (2022), pp. 435–452.

[87] Gracia-Fernández, C. A., Gómez-Barreiro, S., López-Beceiro, J., et al. New approach to the double melting peak of poly (l-lactic acid) observed by DSC. *Journal of Materials Research* 27.10 (2012), pp. 1379–1382.

[88] Harris, L. "A Study of the crystallisation kinetics in PEEK and PEEK composites". PhD thesis. University of Birmingham, 2011.

[89] Perez-Martin, H., Mackenzie, P., Baidak, A., et al. Crystallinity studies of PEKK and carbon fibre/PEKK composites: A review. *Composites Part B: Engineering* 223 (2021), p. 109127.

[90] Wang, P., Zou, B., Xiao, H., et al. Effects of printing parameters of fused deposition modeling on mechanical properties, surface quality, and microstructure of PEEK. *Journal of Materials Processing Technology* 271 (2019), pp. 62–74.

[91] Chacón, J., Caminero, M., Núñez, P., et al. Additive manufacturing of continuous fibre reinforced thermoplastic composites using fused depo-

sition modelling: Effect of process parameters on mechanical properties. *Composites science and technology* 181 (2019), p. 107688.

[92] Heidari-Rarani, M., Rafiee-Afarani, M, and Zahedi, A. Mechanical characterization of FDM 3D printing of continuous carbon fiber reinforced PLA composites. *Composites Part B: Engineering* 175 (2019), p. 107147.

[93] Wang, K., Long, H., Chen, Y., et al. Heat-treatment effects on dimensional stability and mechanical properties of 3D printed continuous carbon fiber-reinforced composites. *Composites Part A: Applied Science and Manufacturing* 147 (2021), p. 106460.

[94] Zhang, M., Sun, B., and Gu, B. Accelerated thermal ageing of epoxy resin and 3-D carbon fiber/epoxy braided composites. *Composites Part A: Applied Science and Manufacturing* 85 (2016), pp. 163–171.

[95] Muna, I. I., Mieloszyk, M., Rimasauskiene, R., et al. Thermal effects on mechanical strength of additive manufactured CFRP composites at stable and cyclic temperature. *Polymers* 14.21 (2022), p. 4680.

[96] Daniel, I. M., Ishai, O., Daniel, I. M., and Daniel, I. *Engineering mechanics of composite materials*. Vol. 1994. Oxford university press New York, 2006.

[97] Behrens, E. Thermal conductivities of composite materials. *Journal of Composite Materials* 2.1 (1968), pp. 2–17.

[98] Hasselman, D. and Johnson, L. F. Effective thermal conductivity of composites with interfacial thermal barrier resistance. *Journal of composite materials* 21.6 (1987), pp. 508–515.

[99] Schapery, R. A. Thermal expansion coefficients of composite materials based on energy principles. *Journal of Composite materials* 2.3 (1968), pp. 380–404.

[100] Chowdhury, N, Wang, J, Chiu, W., and Yan, W. Residual stresses introduced to composite structures due to the cure regime: effect of environment temperature and moisture. *Journal of Composites* 2016.1 (2016), p. 6468032.

[101] Somireddy, M., Czekanski, A., and Singh, C. V. Development of constitutive material model of 3D printed structure via FDM. *Materials Today Communication* 15 (2018), pp. 143–152.

[102] Somireddy, M, Singh, C., and Czekanski, A. Analysis of the material behavior of 3D printed laminates via FFF. *Experimental Mechanics* 59(6) (2019), pp. 871–881.

[103] Simon, J and Jain, A. The Effect of Packing Type on the Equivalent Modulus and Stress Concentrations of Unidirectional Composites. *Mechanics of Composite Materials* 58.6 (2023), pp. 883–896.

[104] Jiménez-Fortunato, I., Bull, D. J., Thomsen, O. T., and Dulieu-Barton, J. M. On the source of the thermoelastic response from orthotropic fibre reinforced composite laminates. *Composites Part A: Applied Science and Manufacturing* (2021), p. 106515.

[105] Noor, A. K., Burton, W. S., and Bert, C. W. Computational models for sandwich panels and shells (1996).